FINAL REPORT

Robust Membranes for Sustainable Wastewater Treatment by Forward Osmosis in FOBs

SERDP Project ER-2217

MAY 2017

Dr. Menachem Elimelech
Yale University

SERDP
DOD ▪ EPA ▪ DOE

Page Intentionally Left Blank

Page Intentionally Left Blank

REPORT DOCUMENTATION PAGE

Form Approved
OMB No. 0704-0188

1. REPORT DATE *(DD-MM-YYYY)*	**2. REPORT TYPE**	**3. DATES COVERED** *(From - To)*
09-05-2017	Final Report	Oct 2014 – May 2017

4. TITLE AND SUBTITLE

Robust Membranes for Sustainable Wastewater Treatment by Forward Osmosis in FOBs

5a. CONTRACT NUMBER
W912HQ-14-C-0039

5b. GRANT NUMBER

5c. PROGRAM ELEMENT NUMBER

6. AUTHOR(S)

Liu, Caihong, Lee, Jongho, Shaffer, Devin, Elimelech, Menachem

5d. PROJECT NUMBER
ER-2217

5e. TASK NUMBER

5f. WORK UNIT NUMBER

7. PERFORMING ORGANIZATION NAME(S) AND ADDRESS(ES)

Yale University
Department of Chemical &
Environmental Engineering
17 Hillhouse Avenue
New Haven, CT 06511

8. PERFORMING ORGANIZATION REPORT NUMBER

9. SPONSORING / MONITORING AGENCY NAME(S) AND ADDRESS(ES)
Strategic Environmental Research and Development Program
4800 Mark Center Drive, Suite 17D03, Alexandria, VA 22350-3605

10. SPONSOR/MONITOR'S ACRONYM(S)
SERDP

11. SPONSOR/MONITOR'S REPORT NUMBER(S)

12. DISTRIBUTION / AVAILABILITY STATEMENT

Approved for public release; distribution is unlimited

13. SUPPLEMENTARY NOTES

14. ABSTRACT
We have developed antifouling TFC membranes for use in the osmotic membrane bio-reactor (OsMBR) to treat wastewaters at forward operating bases. We proposed two different modification strategies, i*n-situ fabrication* and *post-fabrication* membrane modification. *In-situ fabrication* modification involves fabrication of a polyamide selective layer and anchoring jeffamine, a poly(ethylene glycol) derivative. For *post-fabrication* strategy, we modified the surface of commercial TFC-FO membranes by grafting jeffamine, silica nanoparticles (SiNPs), and zwitterionic polymer brushes. The *in-situ fabrication* technique did not exhibit consistent fouling resistance of the fabricated membranes due to the high sensitivity to experimental conditions such as temperature and humidity. We concluded that *in-situ fabrication* technique may not be adequate to produce consistent and reliable fouling resistance of TFC membranes. In contrast, commercial TFC-FO membranes modified by the *post-fabrication* strategy showed an enhanced fouling resistance of the modified TFC membranes in static and dynamic fouling experiments with various foulants, without impacting the intrinsic membrane transport properties. Finally, we employed the developed membrane in a crossflow OsMBR system using return activated sludge as a feedwater. The membrane exhibited a significantly delayed fouling behavior compared to pristine TFC membranes, showing the great promise of the developed antifouling membrane modification technique.

15. SUBJECT TERMS
Wastewater treatment, forward osmosis, membrane bioreactor (MBR), osmotic MBR, membrane fabrication, membrane fouling

16. SECURITY CLASSIFICATION OF:			**17. LIMITATION OF ABSTRACT**	**18. NUMBER OF PAGES**	**19a. NAME OF RESPONSIBLE PERSON**
a. REPORT	**b. ABSTRACT**	**c. THIS PAGE**			Menachem Elimelech
U			SAR	71	**19b. TELEPHONE NUMBER** *(include area code)* 1-203-687-2789

Page Intentionally Left Blank

Table of Contents

List of Tables

List of Figures

List of Acronyms

AFM	Atomic Force Microscopy
APTMS	(3-Aminopropyl)trimethoxysilane
ARGET	Activators Regenerated by Electron Transfer
ATR-FTIR	Attenuated Total Reflectance Fourier Transform Infrared Spectroscopy
ATRP	Atom-Transfer Radical-Polymerization
BiBB	2-Bromo-2-methylpropionyl bromide
BSA	Bovine Serum Albumin
DMF	Dimethylformamide
E.coli	Escherichia coli
EDC	1-Ethyl-3-(3-dimethylaminopropyl)carbodiimide
FO	Forward Osmosis

HCl	Hydrochloric acid
LB	Lysogeny broth
MBR	Membrane Bioreactor
MES	2-(N-morpholino)ethanesulfonic acid
NHS	N-Hydroxysuccinimide
NMP	N-Methyl-2-pyrrolidone
NOM	Natural Organic Matter
ODMP	Osmotically-Driven Membrane Process
OsMBR	Osmotic Membrane Bioreactor
PDA	Polydopamine
PEG	Poly(ethylene glycol)
PEGDE	Poly(ethylene glycol) Diglycidyl Ether
PET	Polyester
PSBMA	Poly(sulfobetaine methacrylate)
Psf	Polysulfone
RAS	Returned Activated Sludge
RMS	Root Mean Square
SBMA	Sulfobetaine methacrylate
SEM	Scanning Electron Microscopy
SiNPs	Silica Nanoparticles
TFC	Thin-film composite
TMAC	Trimethylammonium chloride
TMC	Trimesoyl chloride
TPMA	Tris(2-pyridylmethyl)amine

Keywords

Wastewater treatment, forward osmosis, membrane bioreactor (MBR), osmotic MBR, membrane fabrication, membrane fouling, fouling resistance, internal concentration polarization.

Abstract

Objective. Recent studies have shown that the osmotic membrane bioreactor (OsMBR), a novel concept integrating forward osmosis (FO) separation with biological wastewater treatment, holds promise for transforming wastewater into high-purity water with relatively low energy consumption. The OsMBR system has the potential to be implemented at the Department of Defense's Forward Operating Bases for on-site, cost-effective, and sustainable wastewater treatment. We developed robust membranes with high water flux and low fouling propensity for efficient operation of the OsMBR. The fabricated membranes demonstrate high fouling resistance against both synthetic and real wastewaters containing high loadings of organic foulants.

Technical Approach. We employed two different modification strategies, i.e., *in-situ fabrication* and *post-fabrication* membrane modification. For *in-situ fabrication* modification, the thin-film composite (TFC) membrane was first prepared by interfacial polymerization with 1,3-phenylenediamine (MPD) and 1,3,5-benzenetricarbonyl trichloride (TMC). jeffamine, an amine-terminated poly(ethylene glycol) derivative, was then grafted to the nascent polyamide layer by reaction with surface acyl chloride groups.

For *post-fabrication* strategy, we modified the surface of commercial TFC-FO membranes by grafting three different hydrophilic materials, i.e., jeffamine, silica nanoparticles (SiNPs), and zwitterionic polymer brushes. jeffamine was bound to the membrane surface using a carbodiimide-mediated, amide coupling reaction. SiNP-based modification was performed first by functionalization of SiNPs using silane molecules with amine terminal groups or quaternary ammonium moieties, followed by dip-coating of the TFC membrane with the functionalized SiNPs. Zwitterionic polymer brush layer was grafted on the TFC membranes via surface-initiated atom-transfer radical-polymerization (ATRP).

Results. The *in-situ fabrication* membrane modification, which involves the fabrication of polyamide TFC membrane via interfacial polymerization, exhibited a large variation of transport properties, i.e., water and salt permeabilities. This inconsistency made it difficult to ensure reproducible fouling resistance of the membranes prepared by the *in-situ fabrication* technique. Because commercial TFC-FO membranes possess consistent membrane transport properties, we instead focused on development of *post-fabrication* modification techniques. We assessed antifouling properties of the modified membranes using adsorption tests with representative foulants, including proteins and bacteria, as well as dynamic fouling experiments in forward osmosis with various organic foulants (i.e., bovine serum albumin, sodium alginate, and natural organic matter). Among the developed techniques, the zwitterionic polymer-based modification resulted in the most fouling resistant TFC membrane. The observed excellent fouling resistance was attributed to the exceptional water affinity, net-zero charge, and dense grafting of zwitterionic polymer brushes. Finally, we demonstrated improved fouling resistance of the zwitterionic polymer modified TFC membrane in an osmotic membrane bioreactor using activated sludge.

Benefits. The developed fouling resistant forward osmosis membranes for an OsMBR demonstrated excellent fouling resistance against synthetic and real wastewaters. These antifouling forward osmosis membranes can also be used in seawater and brackish water desalination, in addition to wastewater treatment and reuse. Ultimately, the use of OsMBR for

onsite wastewater treatment at DOD forward operating bases will reduce the need to haul wastewater offsite for treatment and disposal, resulting in economic, environmental, and safety benefits.

Background & Relevant Research

Owing to their lower fouling propensity and potentially lower energy requirements compared to conventional technologies such as reverse osmosis (RO), osmotically-driven membrane processes (ODMPs) hold significant promise in augmenting water supplies using seawater and wastewater [5, 6]. The potential of engineered osmosis in wide-ranging applications, from desalination and wastewater reclamation [7-9], to food processing and protein concentration [10, 11], has recently been demonstrated. ODMPs utilize the osmotic pressure difference created across a semipermeable membrane separating two streams of different concentrations to drive water permeation. Permeation across the semipermeable membrane results in concentration of the more dilute stream, referred to as the feed, and dilution of the more concentrated stream. In particular, the osmotic membrane bioreactor (OsMBR) is a wastewater treatment technology that offers several advantages over conventional membrane bioreactors (MBRs) [12]. In an OsMBR, a semipermeable membrane is immersed in an activated sludge bioreactor that is continuously aerated to supply oxygen for the biomass. Osmosis (hereafter forward osmosis, FO) drives permeation of water from the wastewater feed stream, across the semipermeable membrane, into the concentrated draw solution. The diluted draw solution is directed to a regeneration process (e.g., RO or distillation), which reconcentrates the draw solution and generates product water. Compared to conventional MBRs employing vacuum-driven microfiltration (MF) or ultrafiltration (UF) membranes, the semipermeable FO membrane at the core of the OsMBR achieves much higher dissolved solute rejection [12]. Moreover, osmosis-driven water permeation in the OsMBR has an inherently lower fouling propensity and therefore requires less frequent backwashing [13]. A schematic diagram of the OsMBR is shown in Figure 1.

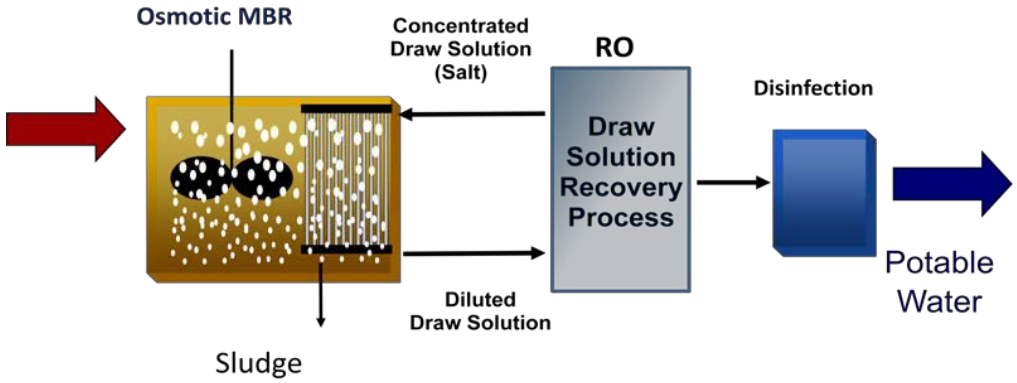

Figure 1. Schematic diagram of an osmotic membrane bioreactor (OsMBR).

The future prospects of the OsMBR depend on the design of an FO membrane tailored to the specific needs of this and other ODMPs. To date, thin-film composite (TFC) membranes are the gold standard for membrane-based water treatment applications including FO due to the exceptional high water permeability and salt rejection of such membranes. These membranes comprise a non-porous, highly crosslinked polyamide selective layer formed through interfacial polymerization of a diamine with a triacyl chloride, and an underlying porous support layer,

typically made of polysulfone. However, the surface physiochemical properties of TFC membranes render them prone to fouling, which is also a major problem affecting state-of-the-art TFC membranes for ODMPs. This technical challenge for ODMPs, though less pronounced in comparison to fouling of RO systems, affects FO membranes treating feed waters with high organic loadings (such as those of OsMBR), thereby decreasing process performance and increasing operating costs due to more frequent cleaning [12].

At the molecular level, fouling originates from the adsorption of organic molecules on a surface for which they have more energetic affinity [14]. In the case of TFC membranes, adsorption followed by fouling occurs because interactions between feed foulants and the hydrophobic surface of the polyamide TFC surface are stronger than foulant-water or polyamide surface-water interactions. Given these foulant-polyamide interactions, one strategy for preventing fouling by foulant adsorption consists of modifying the membrane surface to render it more hydrophilic. This strategy should lead to an anti-fouling surface through a steric barrier for foulant adsorption (through, for instance, grafted polymer brushes) and by increasing surface affinity for water [15, 16]. Studies by Whitesides and collaborators [17, 18] identified poly(ethylene glygol) (PEG) as the building block of anti-fouling polymer grafts. This body of work also identified other structural properties of polymers having potential anti-fouling properties: they should possess hydrogen bond acceptor groups, but not donors, have polar functional groups, and be electro-neutral.

To mitigate membrane fouling, different strategies have been pursued for the modification of the membrane surface, ranging from polymer grafts [19] to physisorption of hydrophilic nanoparticles [20]. Overall, the antifouling modification strategies can be classified into in-situ modification (i.e., incorporating hydrophilic materials during membrane fabrication) or post-modification (i.e., modifying membrane surfaces with hydrophilic materials after membrane fabrication) [21].

In our initial Limited Scope Proposal, we have proposed three different in-situ membrane preparation protocols based on covalent grafting of PEG-like polymers on the membrane active layer. Specifically, we proposed (i) in situ jeffamine protocol, in which a block copolymer of poly(ethylene glycol) and poly(propylene glycol) is grafted on the nascent polyamide active layer immediately after interfacial polymerization; (ii) EDC-NHS-jeffamine protocol, which results in covalent bonding of jeffamine to surface carbonyls through an EDC-NHS mediated amide linkage reaction; and (iii) amino-PEGDE protocol, in which PEGDE, an epoxide PEG derivative, is grafted to an amino-rich polyamide active layer. All these amino-PEG membrane modifications demonstrated enhanced fouling resistance. In the current reported work, besides continuing to expand upon the amino-PEGDE membrane concept proven earlier, we focused on (i) exploring the in-situ *vs*. post-modification methods for antifouling TFC FO membranes to provide more options for implementation of the technology (i.e., membrane fabrication *vs.* module level modification), (ii) optimizing membrane fabrication / modification conditions to achieve higher fouling resistance while maintaining membrane performance (water flux and salt rejection) at high level, (iii) conducting long-term fouling performance tests with a mixture of organic foulants, and (iv) collaborating with ongoing SERDP funded project(s) for testing our antifouling membranes in an osmotic MBR.

Objective

In the context of the SERDP Statement of Need (SON) Number ERSON-12-01 “Development of Sustainable Wastewater Treatment Processes for Forward Operating Bases (FOBs)”, the Osmotic Membrane Bioreactor (OsMBR), an emerging wastewater treatment process, holds significant promise for deployment at installations of interest to the armed forces. The OsMBR is a modular and scalable membrane technology that produces high quality water through a semipermeable membrane configuration. Because water permeation is driven by an osmotic pressure difference (forward osmosis, FO), the OsMBR has a lower energy consumption (provided a suitable draw solute is available) compared to conventional processes such as reverse osmosis (RO), which are driven by hydraulic pressure.

The objective of this project was to develop fouling resistant thin-film composite (TFC) forward osmosis (FO) membranes for OsMBR to treat wastewater in FOBs. We aimed for two specific goals: 1) grafting of hydrophilic materials on TFC membranes to impart fouling resistance, and 2) demonstration of the fouling resistance of the modified membranes against commonly found organic foulants in realistic fouling environments.

In this Technical Report, we present the preparation, characterization, and testing of thin- film composite forward osmosis (TFC-FO) membranes, that could be suitable for implementation in the OsMBR. We have used two different strategies to develop antifouling FO membranes: i*n-situ fabrication* and *post-fabrication* membrane modifications. We have assessed the fouling resistance of the modified membranes to common foulants including proteins, polysaccharides, and natural organic matter, in static adsorption tests as well as lab-scale FO experiments using synthetic wastewater. We have examined the effects of these surface modifications on membrane transport properties, including water permeability, salt rejection, and support layer structural parameter. Through systematic evaluation of membrane fouling resistance, we have determined the most promising membrane modification techniques that lead to the most fouling resistant TFC membrane; that is, the membrane exhibiting the least water flux decline, while maintaining the membrane transport properties. Finally, we have demonstrated the antifouling performance of the developed TFC-FO membrane in an OsMBR using real wastewater.

Materials and Methods

Fabrication of High Performance Thin-film Composite FO Membranes

TFC-FO membrane fabrication comprises two stages: polysulfone support fabrication and active layer synthesis by interfacial polymerization. We have explored three different protocols for fouling mitigation, which we compare to the standard, unmodified polyamide TFC-FO, referred to as the control membrane.

Polysulfone Support Fabrication

Polysulfone supports were prepared by non-solvent-induced phase inversion [2]. A 40-µm-thick non-woven polyester (PET) fabric was used as backing for the polysulfone supports. The fabric was taped to a glass plate using waterproof adhesive tape. Next, a 9.0 wt.-% polysulfone (M_n 22 kDa) solution in dimethyl formamide (DMF) was prepared and stirred for 6 hours until the polysulfone was completely dissolved, and was then stored in a desiccator overnight. The polysulfone supports were fabricated by drawing the polysulfone solution over the PET fabric, using a casting knife. The PET fabric was wetted with 1-methyl-2-pyrrolidinone (NMP) and the casting knife gate height was set to 15 mils (375 µm). The polysulfone casting was then precipitated in a 3 wt.-% DMF aqueous solution for 10 minutes. Polysulfone supports were stored in deionized (DI) water until the preparation of the polyamide active layer by interfacial polymerization. Figure 2 summarizes the main steps of the polysulfone support preparation protocol.

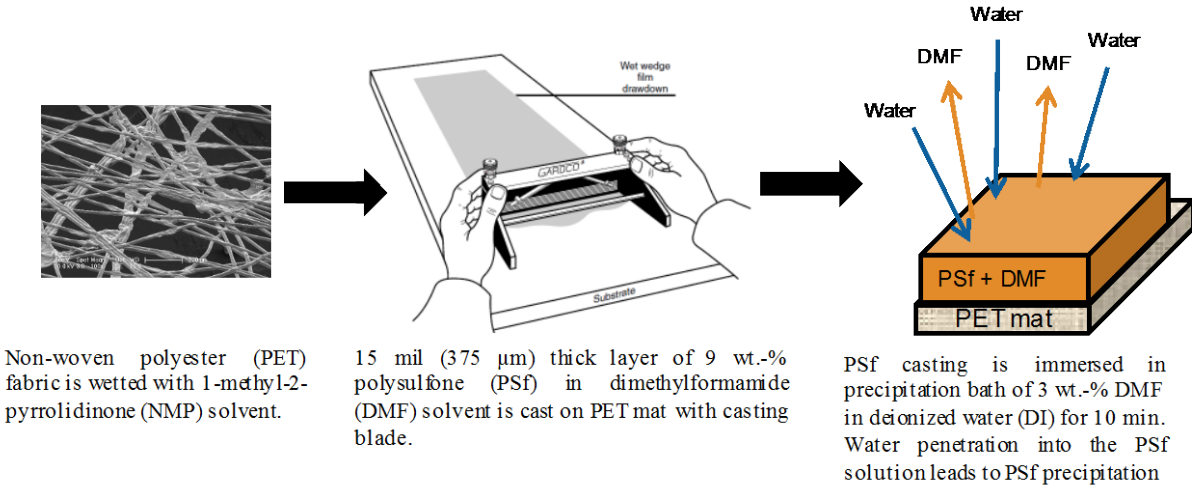

Figure 2. Schematic of the polysulfone support preparation protocol. Adapted from [3].

Figure 3 presents scanning electron micrographs of a representative polysulfone support prepared with this recipe. The micrograph shows that the support microstructure is characterized by fingerlike microvoids that roughly span the complete thickness of the support. The fingerlike morphology is perpendicular to the support surface (i.e., aligned with the direction of permeation).

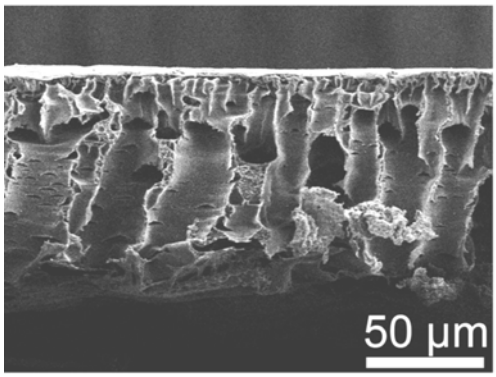

Figure 3. Scanning electron micrograph of a representative polysulfone support layer prepared by non-solvent induced phase inversion [2].

Synthesis of Polyamide TFC-FO Membranes

Control (unmodified) membranes. The selective polyamide layer was prepared following protocols previously reported in the literature [22]. Briefly, the polysulfone support was taped to a glass plate and wetted with an aqueous solution of m-phenylenediamine (MPD, at 3.4 wt.-%) for 2 minutes, after which excess solution was removed with an air knife. Next, the polyamide selective layer (Figure 4) was synthesized by immersing the MPD-saturated support in a 0.15 wt.-% trimesoyl chloride (TMC) solution (in Isopar-G, a proprietary non-polar organic solvent) for 1 minute, followed by drainage of excess TMC for 2 minutes. This was followed by curing of the membrane in deionized (DI) water at 95 °C for 2 minutes, immersion in 200 ppm aqueous sodium hypochlorie (NaOCl) for 2 minutes (to remove excess MPD), and in 1000 ppm sodium bisulfite ($NaHSO_3$) for 30 seconds. Finally, the membrane was cured again in DI water (95 °C) for 2 minutes. All membranes were washed thoroughly and finally stored in DI water at 4°C.

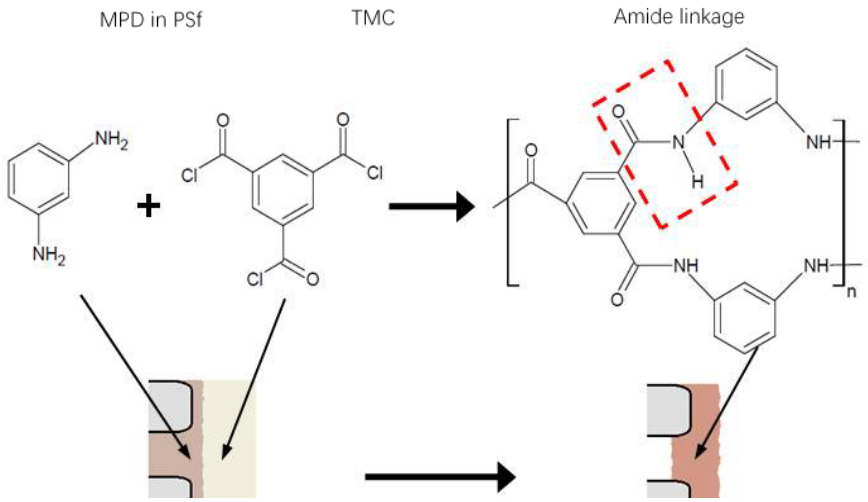

Figure 4. Schematic diagram of the polyamide active layer preparation. Adapted from [3].

In-situ Modification Fouling-resistant Polyamide Membranes

In-situ jeffamine (IS) fouling-resistant polyamide membrane. The *in situ* modification protocol exploits the presence of reactive acyl chloride groups on the nascent polyamide layer in order to covalently bond jeffamine (*O*,*O*′-Bis(2-aminopropyl) polypropylene glycol-*block*-polyethylene glycol-*block*-polypropylene glycol), an amine terminated block copolymer of ethylene glycol and propylene glycol, to the membrane active layer. The molecular structure of jeffamine is presented in Figure 5. This modification protocol was previously applied by Kang et al. [23] to modify RO membranes. To prepare *in situ* jeffamine membranes, the nascent polyamide layer was contacted with 25.0 mL of aqueous jeffamine (molecular weight 1,900 g mol^{-1}) immediately after the post-TMC draining step. This reaction was allowed to proceed for 2 minutes. With the exception of this step, the modification protocol was analogous to that of the control membranes.

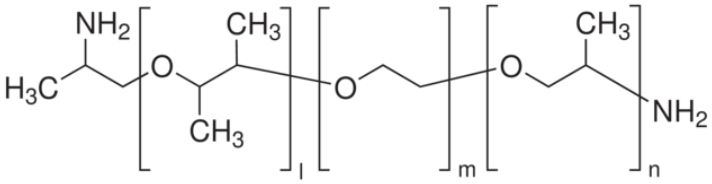

Figure 5. Molecular structure of jeffamine (m ≈ 9; n+l≈ 6). Image credit: Sigma Aldrich.

The in-situ jeffamine (IS) modification protocol is described in Figure 6.

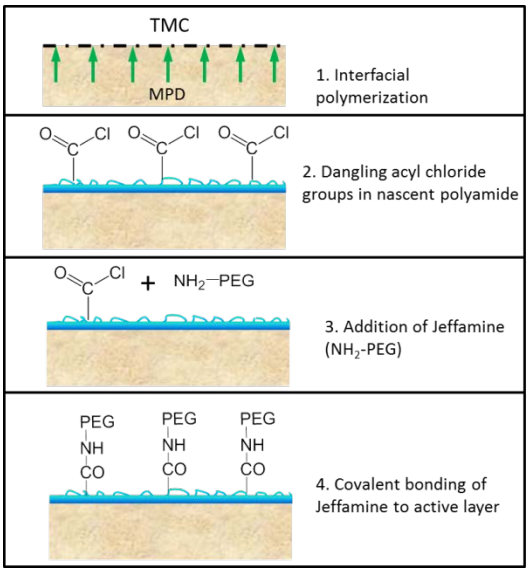

Figure 6. in situ jeffamine membrane preparation scheme

Post Modification Fouling-resistant Polyamide Membranes

Poly(ethylene glycol) block copolymer-modified fouling-resistant membranes. The surfaces of TFC-FO membranes were modified by the attachment of O,O'- Bis(2-aminopropyl) poly(propylene glycol)-block-poly(ethyleneglycol)-block-poly(propyleneglycol). This amine-terminated poly(ethylene glycol) block copolymer is known by the trade name jeffamine (jeffamineED-2003, MW 2000 $gmol^{-1}$, Aldrich), which is registered trademark of the Huntsman Corporation. jeffamine polymer chains were bound to the membrane surface using a carbodiimide-mediated, amide coupling reaction that consisted of two steps, as shown in Figure 7. As illustrated in Figure 7, jeffamine ED-2003 consists of an estimated three repeating units of propylene glycol on each end of repeating units of ethylene glycol.

For the modification procedure, the membranes were clamped onto plastic frames such that the active layer was isolated from the support layer. In the first step of the modification, an activation solution containing 2mM N-(3-Dimethylaminopropyl)-N'-ethyl-carbodiimide (EDC) crosslinker and 5 mM N-Hydroxysuccinimide (NHS, Aldrich) was pipetted over the isolated active layer of the TFC-FO membrane. The activation solution was prepared in DI water buffered at pH 5 with 10 mM 2-(N-Morpholino) ethanesulfonic acid (MES) and containing 0.5 M sodium chloride. EDC in the activation solution reacts with carboxylic groups to form an unstable acylurea inter-mediate, which then reacts with NHS to form a more stable ester. After 10 min contact time, the activation solution was removed. Membrane active layers were rinsed with DI water, and 50 mL of jeffamine solution was pipetted over the active layer.

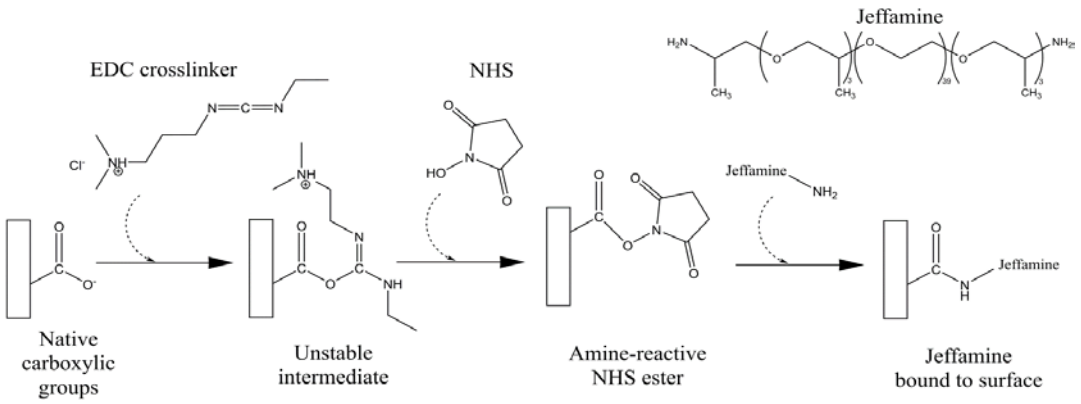

Figure 7. Scheme illustrating jeffamine binding to the membrane surface. Native carboxylic groups on the surface of polyamide thin-film composite membranes are activated by a solution containing N-(3-Dimethylaminopropyl)-N'-ethylcarbodiimide (EDC) and N-Hydroxysuccinimide(NHS). Introduction of a solution containing amine-terminated jeffamine, a poly(ethylene glycol) and poly(propylene glycol) block copolymer, results in nucleophilic substitution of the NHS ester and the formation of an amide bond between the jeffamine polymer and the membrane surface.

jeffamine solutions (wt%) were prepared at concentrations of 1%, 2%, 5%, 10%, and 15% by dissolving jeffamine in DI water containing 0.15 M NaCl and buffered to pH 7.5 with 10 mM 4-(2-Hydro-xyethyl) piperazine-1-ethanesulfonic acid (HEPES). The amine-terminated jeffamine polymer forms an amide bond to the membrane surface by nucleophilic substitution of the NHS ester. Figure 5 illustrates jeffamine attachment via a single amine terminus, but attachment of both ends of the polymer chain may also occur. After 10 min contact with the membrane surface, the jeffamine solution was discarded, and the membrane active layer was rinsed with DI water followed by a rinse with 25% isopropanol. After a final DI water rinse, the jeffamine-modified membranes were stored submerged in DI water in opaque plastic bottles refrigerated at 4 °C.

Silica nanoparticle-modified fouling-resistant membranes. Before coating on the membrane surface, the silica nanopartilces (SiNPs) were functionalized with positively charged ligands. In this work, the functionalization procedures of SiNPs using two different ligands, Trimethylammonium chloride (TMAC) and (3-Aminopropyl)trimethoxysilane (APTMS), are described in our previous publication[24]. Briefly, for TMAC functionalized silica nanoparticles (TMAC-SiNPs), 3 g of Ludox HS-30 colloidal silica were diluted with 22 mL of deionized (DI) water. After sonication for 30 min, 1 M HCl was used to adjust the pH to 5.5. Then, 23 g of TMAC were slowly added while the solution was vigorously stirred. The mixture was stirred at 70 °C overnight to complete the reaction. Subsequently, the functionalized SiNPs suspension was dialyzed in deionized (DI) water using SnakeSkin tubing for 2 days. For APTMS functionalized silica nanoparticles (APTMS-SiNPs), 6 g of Ludox HS-30 colloidal silica were dispersed in 30 mL DI water and sonicated for 30 min. The SiNPs suspension was then added to a mixed solution of 2.22 mL of APTMS and 24 mL of DI water, while the solution was vigorously stirred. pH was adjusted to approximately 5 using 1 M HCl. The final suspension was left on the hot plate at 70 °C overnight and then dialyzed in DI water for 2 days.

The functionalized SiNPs with positive charges were grafted on the TFC forward osmosis membrane through a simple dip-coating (Figure 8). The functionalized SiNP suspension was sonicated for 30 min with pH adjusted to specific values, after which the suspension was left in contact with the active layer of the membrane overnight on a rocking platform at 70 rpm at room temperature (23°C).

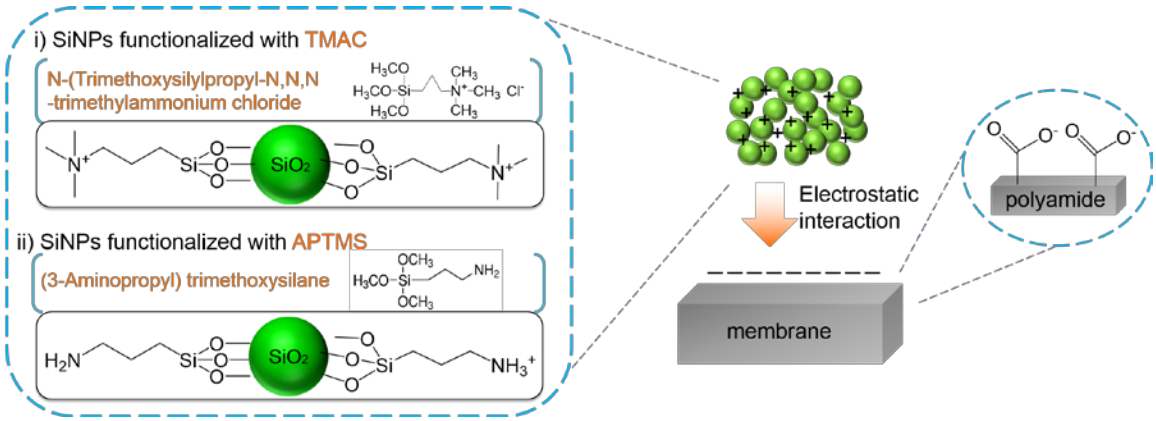

Figure 8. Schematic of TFC membrane modification via surface grafting of functionalized silica nanoparticles (SiNPs). SiNPs were first functionalized by two ligands i) N-(Trimethoxysilylpropyl-N, N, N-Trimethylammonium chloride (TMAC); ii) (3-Aminopropyl) trimethoxysilane (APTMS) through silanization. Then, the positively charged SiNPs are grafted to the negatively charged polyamide TFC membrane by dip-

Zwitterionic polymer-modified fouling-resistant membranes. Dopamine hydrochloride (800 mg, 2.10 mmol) was dissolved in DMF (40 mL) in an amber bottle with a PTFE/silicone septum. After dry nitrogen was bubbled into the solution for 20 minutes, 2-bromoisobutyryl bromide (0.26 mL, 1.05 mmol) and triethylamine (0.3 mL, 1.05 mmol) were added. The solution was then stirred under nitrogen at room temperature for three hours. Meanwhile, a non-modified TFC membrane coupon was sandwiched between a clean glass plate and a rubber mat with a central hole cut out (10 cm × 6.5 cm). A polypropylene frame with the same dimensions as the central hole was combined with the rubber mat and secured by using steel clamps to create a sealed well. The above prepared BiBB-dopamine solution was added to a 200 mL aqueous tris(hydroxymethyl) aminomethane buffer (pH 8.5, 2.0 mmol), which was immediately added into the well to contact the membrane active layer; this step initiates formation of polydopamine (PDA) on the membrane surface. After 10 minutes on a rocking platform at 60 rpm, the membrane was thoroughly rinsed with DI water. The washed membrane (named TFC-PDA hereafter) was stored in aqueous isopropanol (10% v/v) until surface modification.

An SBMA monomer (15.64 g, ~ 56 mmol) was dissolved in a 1:1 volume ratio of isopropanol (IPA):DI water mixture (200 mL, v/v) in a 250 mL glass bottle covered with aluminum foil. After bubbling dry nitrogen through the solution for 10 minutes, 8 mL of copper chloride complex catalyst solution (Copper (II) chloride 0.010 g (14.8 μmol) and Tris(2-pyridylmethyl)amine (TPMA) 0.140 g (0.095 mmol) in 20 mL of 1:1 IPA:DI water (v/v) mixture) were added into the bottle. The prepared TFC-PDA membrane was placed in the 250 mL glass bottle. After bubbling nitrogen for another 10 minutes, 12 mL of the ascorbic acid solution (with a concentration of 1 g in 10 mL of 1:1 IPA:DI mixture) were added to the glass bottle to initiate polymerization. After one hour of polymerization, the bottle was exposed to open air to terminate the ATRP process and the membrane was thoroughly rinsed with DI water. The PSBMA modified membrane (named TFC-PSBMA hereafter) was then stored at 4 °C in aqueous isopropanol (10 v/v %). A schematic diagram for the membrane modification process is shown in Figure 9.

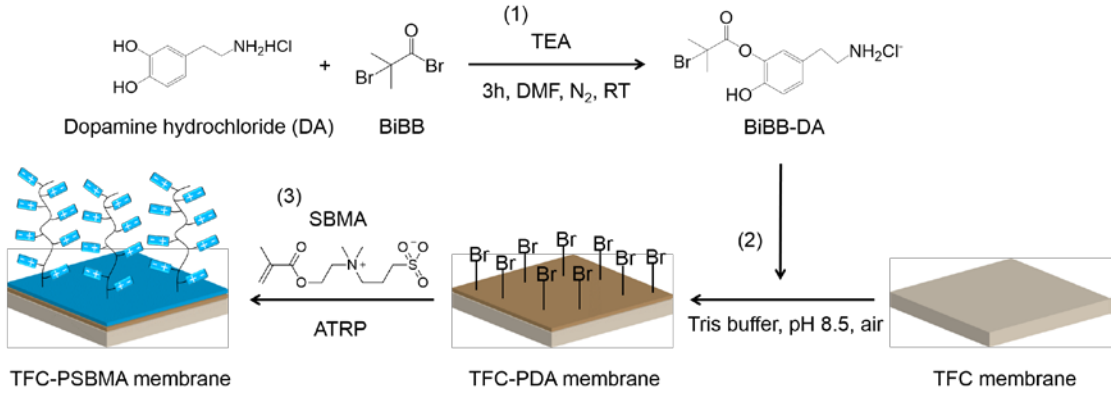

Figure 9. Schematic illustration of TFC membrane modification by grafting zwitterionic polymer brush layer on the membrane surface. (1) Coupling of initiator and dopamine hydrochloride (i.e., BiBB-DA). (2) Immobilization of initiators on the TFC membrane via polymerization of BiBB-DA (i.e., TFC-PDA membrane). (3) Grafting of zwitterionic polymer brush via ATRP (i.e., TFC-PSBMA membrane). BiBB stands for α-bromoisobutyryl bromide, TEA stands for triethylamine, SBMA stands for [2-(methacryloyloxy)-ethyl]dimethyl-(3-sulfopropyl)ammonium hydroxide (also named sulfobetaine methacrylate), and PSBMA stands for poly(sulfobetaine methacrylate).

Surface Characterization

SEM, AFM surface roughness and ATR-FTIR measurements. Scanning electron microscopy (SEM) was used to characterize the membrane surface morphologies before and after modifications.

Membrane surface roughness was measured using an atomic force microscope (AFM) in tapping mode. Symmetric silicon probes (30-nm-thick back side aluminum coating, 40 N/m spring constant, resonance frequency of 300 kHz, tip radius of 8 ± 4 nm) were employed in the measurements. Air-dried membranes were scanned in air at a minimum of 6 randomly selected locations.

Attenuated total reflectance Fourier transform infrared spectroscopy (ATR-FTIR) was used to determine the presence of zwitterionic monomers on the modified membrane surfaces.

Contact angle measurements. The hydrophilicity of control and modified membrane active layers was evaluated by measuring the contact angle of 2-μL sessile DI water droplets using an optical tensiometer. Membrane samples were air-dried for at least 24 hours prior to measurement. Typically, 10 different sessile droplets were photographed on randomly chosen locations over the membrane active layer. The left and right contact angles were determined through video contact angle software, and the data were averaged.

Zeta potential measurements. Zeta potentials of the membrane surface were determined from streaming potential measurements with a background electrolyte of 1 mM KCl and 0.1 mM $KHCO_3$.

Membrane transport and structural parameters measurements Water permeability coefficient (A), salt permeability coefficient (B), and structural parameter (S) of pristine and modified membranes were determined by the FO four-step characterization method described elsewhere [4].

Characterization of Antifouling Performance

Static adhesion tests. Membrane antifouling properties were evaluated by static adsorption tests of bovine serum albumin (BSA) and *Escherichia coli* (*E. coli*). A fluorescein-conjugated BSA (FITC-BSA) (Life Technologies, A23015) at a concentration of 0.05 mg/mL was prepared in a phosphate-buffer saline (PBS) solution at pH 7.4. A membrane coupon (2.1 cm in diameter) was cut and mounted in a custom-made membrane cell holder. FITC-BSA solution (3 mL) was added to the cell holder and left in contact with the membrane active layer (salt rejecting side) in the dark on a rocking platform at 60 rpm for three hours. The solution was then removed and the membrane was gently rinsed twice with PBS buffer. The rinsed membrane coupon was placed on a glass slide with a droplet of PBS buffer on top, covered by a coverglass, with nail polish on the edges for sealing. Fluorescence images were taken by an inverted Axiovert 200 M epifluorescence microscopy (Carl Zeiss Inc., Thornwood, NY, USA).

Membrane adhesion property for bacteria was assessed using plate counting. *E. coli* (ATCC BW26437, Yale Coli Genetic Stock Center, New Haven, CT) cells were cultured in a Lysogeny broth (LB) overnight at 37 °C. After being diluted 25 times with a fresh LB media, the overnight cultured bacterial cells were cultivated to a log phase by growing for about two hours at 37 °C with agitation, at which ~10^9 colony-forming units (CFU)·mL^{-1} were found. The cultures were then washed three times with a sterile 0.9 wt% NaCl solution to remove excess macromolecules present in the growth media, and resuspended in a sterile 0.9 wt% NaCl solution at a final concentration of ~10^9 CFU·mL^{-1}. Finally, a bacterial suspension in a 0.9 wt% NaCl solution at 10^8 CFU·mL^{-1} was prepared for subsequent static adsorption experiments.

Membrane coupons with an area of ~3.5 cm^2 were punched and mounted in custom-made membrane holders. An aliquot of the bacterial suspension (3 mL, 10^8 CFU·mL^{-1}) was added into each holder and kept in contact with the membrane active layer for three hours at room temperature. After exposure, the membranes were rinsed twice with 0.9 wt% NaCl to remove the unattached bacteria. The membrane coupons were then transferred into 50-mL Falcon tubes containing 10 mL of 0.9 wt% NaCl solution and sonicated for 10 minutes to remove the attached bacteria cells from the membrane surface. The supernatant was sequentially diluted, spread on LB agar plates, and incubated at 37 ^oC overnight. After incubation, the grown colonies were counted to quantify the attached bacteria cells on the membranes expressed as CFU·$mL.^{-1}$

Dynamic fouling experiments. Dynamic fouling experiments were conducted in a laboratory-scale FO unit [1]. A schematic diagram of the experimental setup is shown in Figure 10. The flow cell consisted of feed and draw compartment channels with dimensions 77 mm x 26 mm x 3 mm operated without spacers in co-current flow. Variable speed gear pumps were used to pump the feed and draw solution flows in a closed loop. The feed solution container was stirred with a magnetic stirrer. The draw solution container was placed on a digital scale; changes in the weight of the draw solution were logged to a computer in order to calculate the permeate water flux. The feed and draw solution temperature were maintained at 25 °C by heat exchanger coils immersed in a constant temperature water bath.

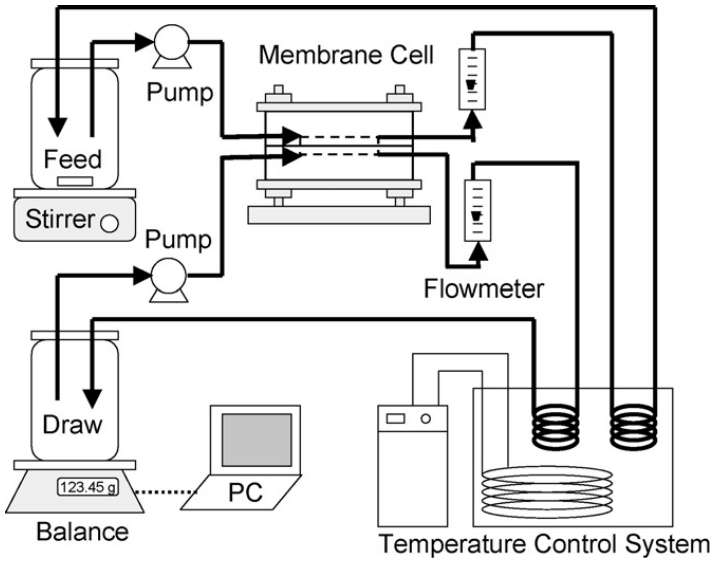

Figure 10. Schematic diagram of the FO experimental setup[1].

The feed solution consisted of organic foulants (i.e., 200 ppm sodium alginate, or combined 100 ppm BSA + 100 ppm sodium alginate + 100 ppm SRNOM) dissolved in synthetic wastewater containing KH_2PO_4 (0.45 mM), NaCl (9.2 mM), $MgSO_4$ (0.61 mM), $NaHCO_3$ (0.5 mM), $CaCl_2$ (0.5 mM), and NH_4Cl (0.93 mM) at pH ~7.4. The synthetic wastewater composition is

representative of secondary effluents of selected wastewater treatment plants in California [25]. Sodium chloride draw solutions (ranging between 1 M and 4 M) were used to generate initial permeate water fluxes of ~20 L m^{-2} h^{-1} (LMH) (the measured initial water flux ~20 LMH). A spacer was used to support the membrane (support layer side) in the draw solution channel. The cross-flow velocity of the draw solution was 4.25 cm/s while the feed solution crossflow velocity was 9.56 cm/s.

Dynamic fouling experiments consisted of two stages. First, a baseline experiment was conducted with a foulant-free feed solution (containing the inorganic solutes at the concentrations given above) to measure the extent of flux decline derived exclusively from draw solution dilution and reverse draw solution diffusion. Next, the fouling experiment was conducted (with foulants present in the feed) at the same initial flux as the baseline experiment. In this case the flux decline observed is due to the combined effect of draw solution dilution, draw solute reverse diffusion and membrane fouling. The baseline and fouling experiments were progressed until a cumulative permeate volume of 500 mL was collected. Water flux decline only due to fouling was then attained by subtracting the baseline (i.e., without foulants) from the measured water flux (i.e., with foulants).

Adhesion force measurements by atomic force microscopy (AFM). The nano-scale adhesion forces determined by AFM contact mode measurements have been shown to be excellent correlators of the fouling propensity of membrane surfaces [1, 14]. We employed the measurement protocol developed by Li and Elimelech [14] to establish the extent to which active layer surface modification decreases the interaction energy between membrane surfaces and a carboxyl-modified latex (CML) particle. The latter, possessing a surface rich in carboxylates, constitutes an appropriate surrogate for organic foulants such as alginate [1]. Adhesion force measurements were performed in a multimode AFM operating in contact mode. A 4-μm CML particle was glued to the tip of a SiN cantilever (spring constant of 0.06 N/m) using optical adhesive, and subsequently cured for 20 minutes in a UV cleaner. A ~0.5-cm^2 clean membrane sample was cut from a wet membrane coupon and taped to a sample holder. A laboratory glass slide to be used for cantilever deflection calibration was taped adjacent to the membrane on the sample holder. Subsequently, the liquid cell, fitted with the functionalized cantilever, was loaded onto the AFM stage, and a silicon rubber o-ring underneath the cell created a seal between the membrane-glass sample and the liquid cell. The liquid cell was filled with ~2 mL testing solution (PBS buffer, or 50 mM NaCl + 0.5 mM $CaCl_2$). After stabilizing the deflection setpoint of the instrument (0 V) for 1 hour, the cantilever deflection sensitivity was calibrated on the glass surface by measuring the slope of the cantilever deflection during piezo retraction. Subsequently, the cantilever was displaced towards the membrane surface for adhesion interaction measurements. Adhesion force measurements were determined from the cantilever deflection during piezo retraction. At least 120 retraction events were recorded for every sample, distributed over 5 randomly chosen locations on the membrane surface.

Side-stream OsMBR using real wastewater (returned activated sludge). Fouling resistance of modified TFC membranes was demonstrated in a side-stream type of OsMBR system via a collaborative work with Professor Amy Childress at University of Southern California. In the side-stream type, a bioreactor contains feedwater (i.e., wastewater). The feedwater is transferred

to a separate forward osmosis unit and water is reclaimed via osmotic pressure difference across a TFC membrane. As a source of real wastewater, a 300 L of returned activated sludge (RAS) has been obtained from Hyperion wastewater treatment plant in Los Angeles, California. The RAS was introduced into the bioreactor as a feed solution.

The cross-flow velocity of the draw and feed solutions was set to be 20 cm/s and the solution temperature was maintained at 30.0 ± 1.0 °C. Each OsMBR test was first operated with 1L of NaCl feed solution prepared to have the same conductivity as the RAS. Based on the initial conductivity of the activated sludge, 1.73 mS/cm, the concentration of the NaCl draw solution was adjusted to result in approximately 10 LMH of water flux. After 1 hour, the feed was switched to an aerated bioreactor containing 15 L of activated sludge from Hyperion wastewater treatment plant. During this stage the activated sludge was kept at a constant volume by replenishment with primary effluent from Hyperion. The membranes were allowed to foul until a steady state water flux was reached. The fouling experiment took approximately 20 hours. The draw solution concentrations were held constant throughout the experiment by automatic dosing based on conductivity measurements. A schematic diagram of side-stream OsMBR for the fouling experiments is shown in Figure 11.

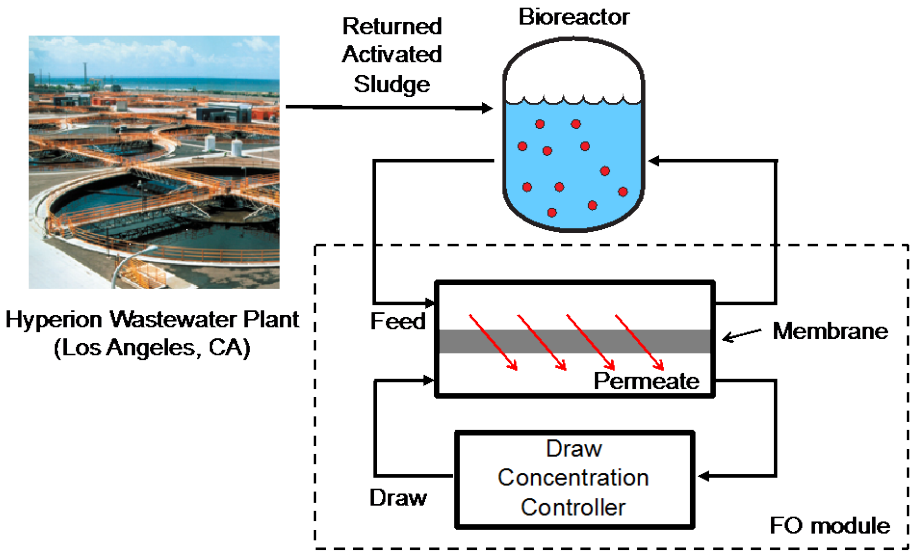

Figure 11. Schematic of side-stream OsMBR for fouling experiments. Returned activated sludge (RAS) was obtained from Hyperion wastewater plant as a feedwater. RAS was first introduced into the reactor, and was provided to a feed side of forward osmosis module. Draw solution concentration was automatically adjusted to maintain a constant osmotic pressure during experiments.

Results and Discussion

In-situ Fabrication Membrane Modification

For in-situ modification, we first fabricated a TFC membrane as an experimental control. A microporous polysulfone support-layer was fabricated by phase inversion, followed by interfacial polymerization to create a thin polyamide selective layer. However, we found that the membrane properties were greatly affected by the environmental/experimental conditions, such as humidity, temperature, and contact time between the membranes and solvent. As a result, the water and salt permeabilities of the fabricated membranes varied significantly from batch to batch (Figure 12). After extensive membrane fabrication efforts, we concluded that the in-situ modification could not lead to consistent membrane properties, mainly due to our manual protocol of membrane hand-casting compared to utilizing industrial automated membrane casting/fabrication machines.

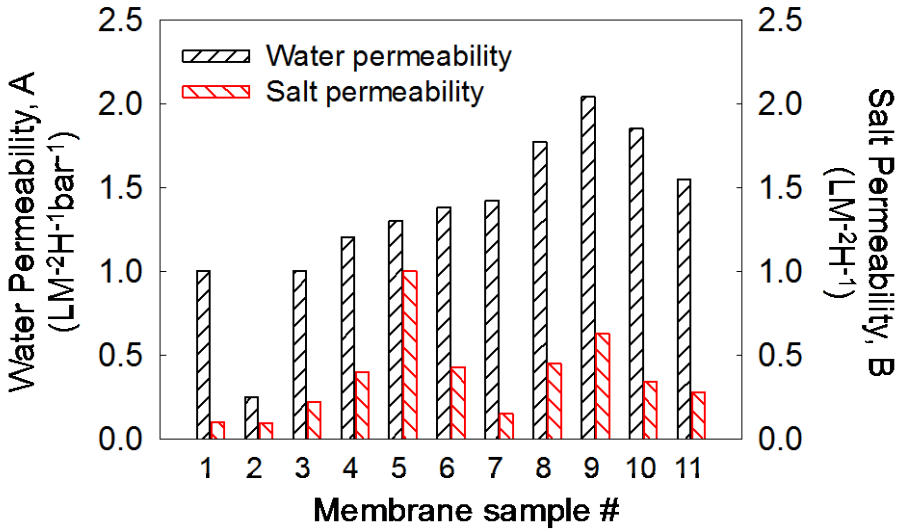

Figure 12. Water and salt permeability of fabricated control polyamide TFC membranes for in-situ modification. Numbers in x axis indicate sequences of the fabricated membranes. The results highlight the difficulty in controlling the properties of fabricated membranes by in-situ modification.

Post-Fabrication Membrane Modification

Membrane Modification Using Jeffamine

Characterization of membrane transport properties. jeffamine grafting reduced the membrane water permeability (*A*) for all jeffamine concentrations used in the membrane modification procedure. The membrane transport properties are summarized in Figure 13. Reductions in water permeability for modified membranes compared to the unmodified control are statistically

significant (significance level α=0.05) for 1%, 5%, 10%, and 15% jeffamine membranes, as determined by a two-sided t-test. This reduction in water permeability for modified membranes is attributed to an increased resistance to mass transport caused by the grafted jeffamine layer. Similar reductions in water permeability or pure water flux have been observed for attachment of jeffamine [26] and other PEG derivatives [27, 28] to commercial polyamide NF and RO membranes and to TFC-FO membranes [29, 30]. Membrane salt permeability (*B*) and salt

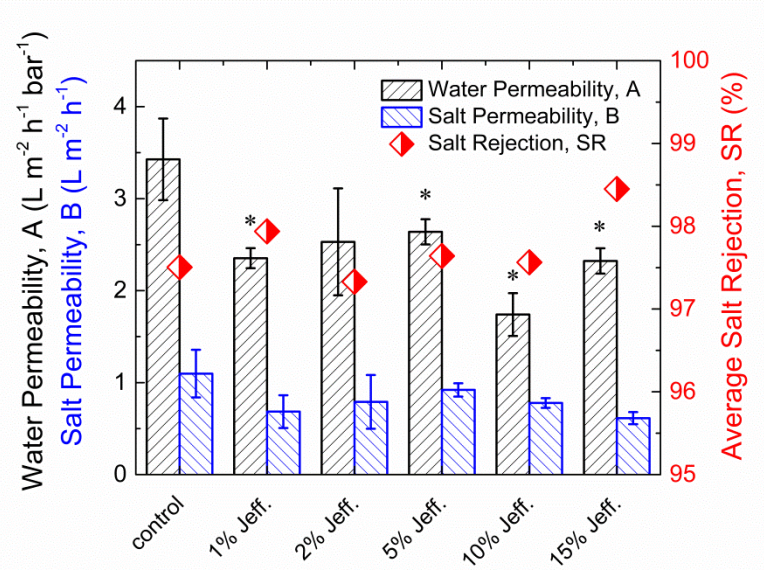

Figure 13. Water permeability coefficients (*A*, L m^{-2} h^{-1} bar^{-1}), salt permeability coefficients (*B*, L m^{-2} h^{-1}), and salt rejection (*SR*, %) of the control and jeffamine (Jeff.)-modified membranes, as measured by reverse osmosis testing. Bars and symbols represent the mean of 2-4 separate tests of different membrane coupons for each membrane type. Error bars extend to one standard deviation. Significant differences between values for the jeffamine-modified membranes compared to the unmodified control membranes are indicated by '*' symbol and were determined in a two-sided t-test at a significance level α=0.05.

rejection (*SR*) were not significantly affected by jeffamine grafting, and preservation of high salt rejection indicates that the grafting method does not damage the membrane active layer.

Hydrophilicity. Changes in membrane surface hydrophilicity were assessed by water contact angle. Previous work on surface modifications for polyamide RO [28] and FO [29, 30] membranes has demonstrated that reduced water contact angle is a reliable indicator of PEG attachment. More hydrophilic membrane surfaces have been correlated with improved membrane fouling resistance [31, 32]. Specifically, for TFC-FO membranes, recent work has demonstrated that hydrophilic surface modifications reduced the extent of organic fouling for modified membranes compared to unmodified controls [29, 30]. Consequently, water contact angle measurements were used as an indicator of both jeffamine grafting and associated membrane fouling resistance.

Significant reductions in water contact angle were observed for the jeffamine-modified membranes compared to the unmodified control membranes (two-sided t-test, α=0.05), suggesting an improvement in the fouling resistance of the modified membrane surfaces. The

distributions of water contact angles measured for each membrane modification condition are shown in Figure 14. The mean water contact angle decreases with increasing jeffamine concentration for membranes modified with 1%, 2%, and 5% jeffamine. However, further reductions in mean water contact angle are not observed for membranes modified with jeffamine concentrations greater than 5% jeffamine.

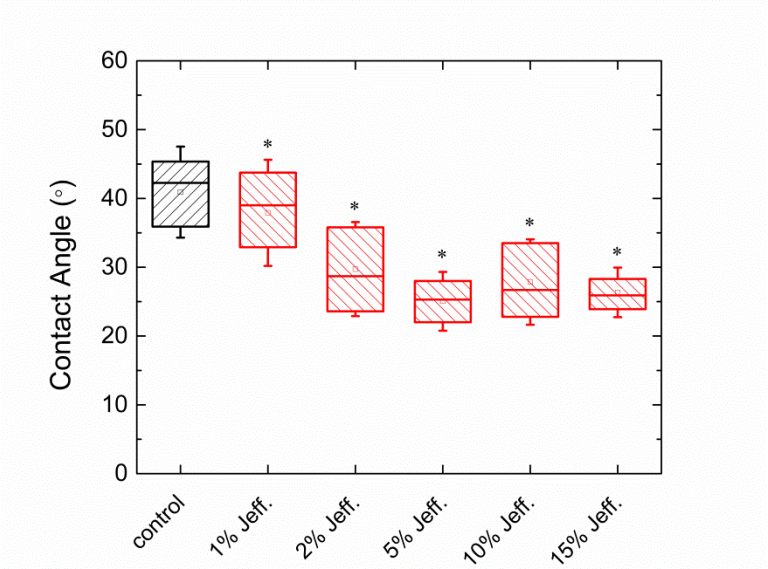

Figure 14. Comparison of measured water contact angles for unmodified control membranes and membranes modified with different concentrations of jeffamine (Jeff.) solution. Boxes represent the 25th, 50th, and 75th percentile values for a distribution of at least 72 contact angle measurements on 2-3 coupons of each membrane type. Whiskers extend to one standard deviation, and square symbols inside the boxes indicate the mean contact angle. The '*' symbol denotes that water contact angles for all jeffamine-modified membranes are significantly less than the contact angles of the unmodified control membrane, as determined by two-sided t-tests at a significance level α=0.05.

Degree of jeffamine grafting. ATR-FTIR spectra were measured for jeffamine-modified membranes and compared to the spectra of unmodified control membranes as another qualitative indicator of jeffamine attachment. Spectra show characteristic bands of the membrane polyamide active layer and the underlying polysulfone support layer due to the relatively large penetration depth of the IR [33]. The degree of grafting may be calculated from ATR-FTIR spectra as a parameter to facilitate the comparison of different membrane modification conditions. Degree of grafting is defined as the ratio of absorbance at a wavenumber indicative of the grafted polymer to absorbance at a wavenumber that is indicative only of the unmodified membrane and that is not affected by the presence of the modifying agent [34]. Spectral changes at wavenumber 1080 cm^{-1} are commonly used to assess PEG grafting to polyamide membranes and are attributed to the C-O and C-C stretch of poly(ethylene glycol) [26, 27, 29, 30, 35]. Accordingly, degrees of jeffamine grafting were calculated from ATR-FTIR spectra as the ratio of jeffamine absorbance at wavenumber 1080 cm^{-1} ($A_{1080cm-1}$) to polyamide absorbance at reference wavenumber 1150 cm^{-1} ($A_{1150cm-1}$) or 1170 cm^{-1} ($A_{1170cm-1}$), which are attributed to symmetric C-SO_2-C stretching in the polysulfone support layer [36, 37].

Figure 15(A) includes representative ATR-FTIR spectra for an unmodified control TFC-FO membrane and a jeffamine-modified membrane. Degrees of jeffamine grafting calculated at both 1150 cm^{-1} and 1170 cm^{-1} reference wavenumbers are shown in Figure 15(B). Statistically significant increases in the calculated degrees of jeffamine grafting (two-sided t-tests, α=0.05) were observed for membranes modified at 2%, 5%, 10%, and 15% jeffamine compared to the unmodified control. The calculated degrees of grafting at 2%-15% jeffamine are not statistically different, indicating no additional jeffamine grafting to the membrane surface occurs at concentrations greater than 2% jeffamine.

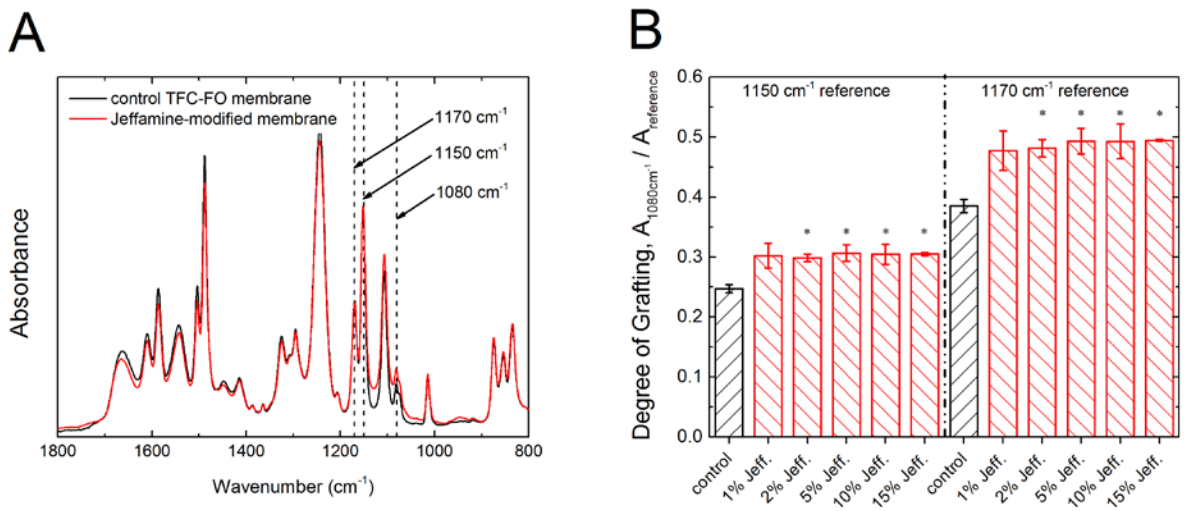

Figure 15. A) Representative attenuated total reflectance-Fourier transform infrared (ATR-FTIR) absorbance spectra for an unmodified control thin-film composite forward osmosis (TFC-FO) membrane and a jeffamine-modified membrane. Absorbance peaks at wavenumbers 1150 cm^{-1} and 1170 cm^{-1} are attributed to the membrane polysulfone support layer (C-SO_2-C stretch), and an increase in the absorbance peak at wavenumber 1080 cm^{-1} is attributed to the presence of grafted jeffamine on the modified membrane surface (C-O and C-C stretch). B) Comparison of degrees of grafting for membranes modified at different jeffamine (Jeff.) solution concentrations and unmodified control membranes. Degrees of grafting were calculated from ATR-FTIR spectra as the ratio of absorbance at 1080 cm^{-1} ($A_{1080\ cm\text{-}1}$) to absorbance at either 1150 cm^{-1} or 1170 cm^{-1} ($A_{reference}$). Bars represent the mean degree of grafting calculated from spectra collected for two different membrane samples. Error bars extend to one standard deviation. Significant differences between the degree of grafting for jeffamine-modified membranes compared to the unmodified control are indicated by a '*' symbol and were assessed by a two-sided t-test at significance level α=0.05.

Charge density. Successful jeffamine binding to the membrane surface reduces the number of native carboxylic groups. Thus, reduced carboxylic group densities for the jeffamine-modified membranes compared to the unmodified control membrane are attributed to the grafting of jeffamine to this fraction of carboxylic groups. Figure 16 presents the results of two TBO dye tests quantifying the densities of carboxylic groups for a set of control, 2% jeffamine-modified, and 15% jeffamine-modified membranes. Compared to the unmodified control membranes, the mean reductions in calculated carboxylic group densities for the 2% jeffamine membranes are ~7% and ~2%. No difference in the carboxylic group surface densities is observed for membranes

modified at 2% and 15% jeffamine concentrations, further indicating that no additional jeffamine grafting occurred for membrane modifications performed at concentrations greater than 2%.

Optimal concentration for membrane modifications. Based on the transport properties and

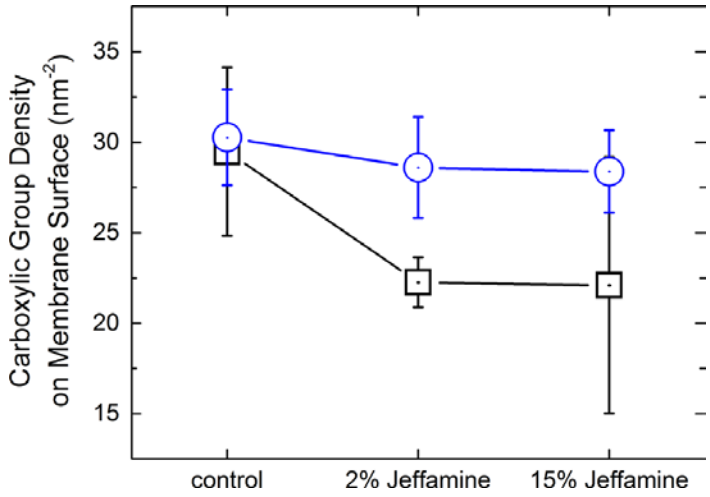

Figure 16. Comparison of carboxylic group surface densities for control and jeffamine-modified membranes, calculated from the results of Toluidine Blue O (TBO) electrostatic dye tests. Blue circles and black squares represent separate dye tests, each performed on samples of unmodified control membranes and membranes modified at 2% jeffamine and 15% jeffamine concentrations. Each test was conducted on three coupons of each membrane type, and eight measurements were collected for each membrane coupon. Symbols represent the mean carboxylic group density calculated from 24 measurements, and error bars extend to one standard deviation.

surface characteristics of the modified membranes discussed in the previous subsections, we identified 2% jeffamine as the optimal solution concentration for membrane modification. A 2% jeffamine solution concentration achieves the apparent maximum grafting of jeffamine to the membrane surface and the associated maximum reduction in water contact angle. Membranes modified with 2% jeffamine demonstrate an acceptable reduction in water permeability compared to the unmodified control membrane and the membranes modified at other jeffamine solution concentrations. Experiments investigating the organic fouling resistance of modified membranes were conducted with membranes modified with this optimal 2% jeffamine concentration.

Confocal imaging of labeled jeffamine membranes. Confocal microscopy images of the surfaces of membranes modified with Rhodamine-labeled jeffamine were analyzed and compared to those of unmodified control membranes. The confocal images demonstrate that jeffamine attachment to the membrane surface is non-uniform with distinct micrometer-scale areas of jeffamine on the membrane surface, as shown in the representative image in Figure 17(A). The control membrane exhibited no fluorescence, confirming that the Rhodamine-labeled

jeffamine was the source of the red fluorescence for the modified membranes. For the 16 membrane images analyzed, the mean surface coverage of Rhodamine-labeled jeffamine was less than 1% of the membrane area.

Rhodamine-labeled jeffamine was also used in our recent study [29] to examine the extent of jeffamine coverage on membrane surfaces modified in situ during fabrication. The in situ modified membranes, for which jeffamine was grafted to acyl chloride groups in the nascent polyamide layer, showed mean surface coverage by rhodamine-labeled jeffamine that was an order of magnitude greater than the jeffamine-modified membranes presented in this work. The greater extent of jeffamine coverage for the in situ modified membranes versus these post-fabrication modified membranes suggests that a higher grafting density is achievable when jeffamine is grafted to acyl chloride groups in situ rather than after membrane fabrication, at which point acyl chloride groups have been hydrolyzed to carboxylic groups, and EDC-NHS is necessary to mediate the jeffamine grafting.

Other studies have similarly observed low surface grafting density when PEGylating polyamide membranes using post-fabrication techniques that rely on available surface functional groups as grafting sites [26, 27]. The mass of PEG that could be grafted to RO membranes was limited for large PEG polymers (MW 1,000 g mol^{-1}), with similar membrane properties observed for membranes modified with 1% and 15% PEG solutions [27]. For jeffamine grafting to RO membranes, polymer chain length appeared to affect grafting density. Larger polymer chains were theorized to exert a steric effect that repulsed other polymer chains and resulted in a lower grafting density compared to the density of smaller jeffamine polymer chains [26]. For the EDC-NHS mediated jeffamine modifications in this work, confocal microscopy images combined with TBO dye test results suggest that not all carboxylic groups on the membrane surface have been grafted with jeffamine, resulting in non-uniform, low-density surface coverage. The unreacted sites may represent surface carboxylic groups that are inherently inaccessible in the polyamide layer, which is estimated to be 20-60% of carboxylic groups [38], or these carboxyl groups may have been shielded from jeffamine grafting because of a steric effect from adjacent grafted jeffamine polymers.

***Surface roughness*.** Surface roughness measurements for the 2% jeffamine modified membranes and unmodified control membranes also demonstrate the non-uniformity of jeffamine attachment. The surface roughness for 2% jeffamine membranes, represented by root mean square roughness (*RMS*, nm), is significantly greater than the roughness of unmodified control membranes (two-sided t-test, α=0.05), as shown in Figure 17(B). *RMS* roughness is the square root of the mean of squared roughness values measured for each 100 μm^2 measurement area, and it represents the deviation of surface peaks and valleys from the mean height plane [39].

Increases in surface roughness have been reported for other post-fabrication PEG membrane modifications [26-28], though a dependence on the initial roughness of the unmodified membrane surface has also been observed [34]. Increased surface roughness was also observed for PEG grafting to acyl chloride groups in the nascent polyamide layer of RO membranes during fabrication [35]. However, using a similar technique to modify polyamide FO membranes in situ resulted in a decrease in membrane surface roughness [29]. The different reported effects of PEG modifications on membrane surface roughness may be interpreted as a function of PEG grafting density. When high density is achieved, PEG chains form a uniform polymer brush that diminishes surface roughness features. However, low-density or non-uniform grafting causes localized areas of increased height that exaggerate overall surface roughness. For the 2% jeffamine-modified membranes, the increase in surface roughness compared to the control membranes is attributed to the non-uniform jeffamine attachment that was observed by fluorescence microscopy. Where micrometer-scale areas of relatively dense jeffamine grafting occurred, local peaks were created that increased the *RMS* roughness.

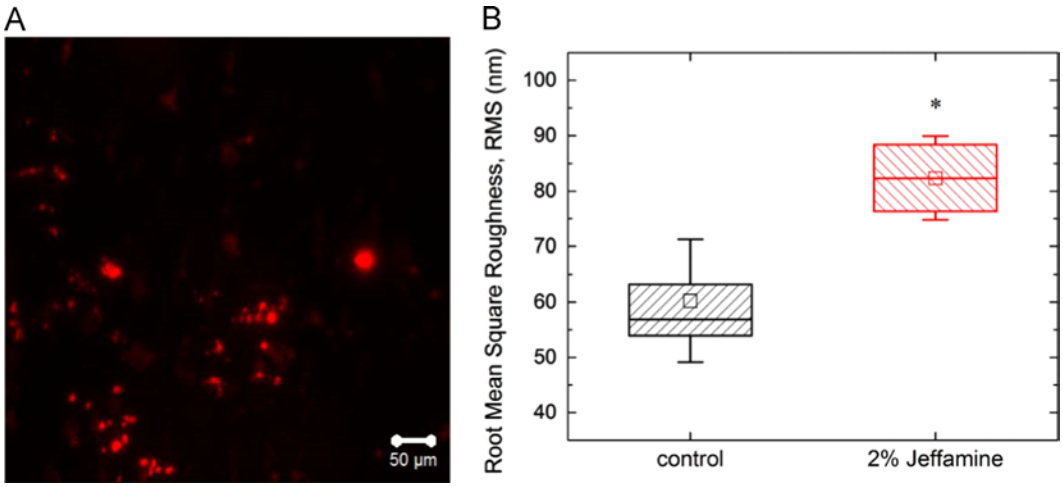

Figure 17. Membrane characteristics indicating the non-uniform attachment of jeffamine to the modified membrane surface. A) Confocal microscopy image of a representative membrane sample that was modified with Rhodamine-labeled jeffamine solution at 2% concentration. Red fluorescence of the Rhodamine dye (excitation at 550 nm and emission observed at 610 nm) demonstrates the non-uniform binding of jeffamine to the membrane surface. B) Comparison of root mean square roughness (*RMS*, nm) for unmodified control membranes and membranes modified with 2% jeffamine solution. Boxes represent the 25th, 50th, and 75th percentile values for a distribution of at least four *RMS* measurements on two coupons of each membrane type. Whiskers extend to one standard deviation, and square symbols inside the boxes indicate the mean sample *RMS* roughness. The '*' symbol denotes that *RMS* roughness for 2% jeffamine-modified membranes is significantly greater than the *RMS* roughness of the unmodified control membranes, as determined by a two-sided t-test at a significance level α=0.05.

Permeate flux decline due to organic fouling. Flux decline in the organic fouling experiments occurs due to both the accumulation of foulants on the membrane surface and the draw solution dilution and feed solution concentration that result from batch operation of the FO test system. The accumulated foulant cake layer creates a physical resistance to water permeation as well as

decreasing the driving force for permeation through cake-enhanced osmotic pressure [40]. Permeate flux decline in the baseline portion of the fouling experiment is attributed only to the effects of batch mode operation, and it enables the contribution of organic fouling to flux decline observed in the subsequent fouling portion of the experiment to be uniquely identified. For each organic fouling experiment, the flux decline due to organic fouling after 500 mL of permeate (FD_{500mL}, %) was calculated as

$$FD_{500mL} = \frac{\left|\left(\frac{J_{w,f}}{J_{w,0}}\right)_{baseline} - \left(\frac{J_{w,f}}{J_{w,0}}\right)_{fouling}\right|}{\left(\frac{J_{w,f}}{J_{w,0}}\right)_{baseline}}(100) \qquad \text{Eq. (1)}$$

where $J_{w,0}$ is the initial water flux, and $J_{w,f}$ is the final water flux after 500 mL permeate has been collected. FD_{500mL} ranges from 0-100% where 0% represents no observed difference between flux decline in the baseline and fouling experiments, and thus no flux decline due to organic fouling. An FD_{500mL} value of 100% represents complete loss of permeate flux in the fouling experiment.

jeffamine-modified membranes experience less flux decline due to organic fouling compared to unmodified control membranes when treating a mixed foulant feed solution, as shown in Figure16. With NaCl draw solution, the mean FD_{500mL} for jeffamine-modified membranes is 11%

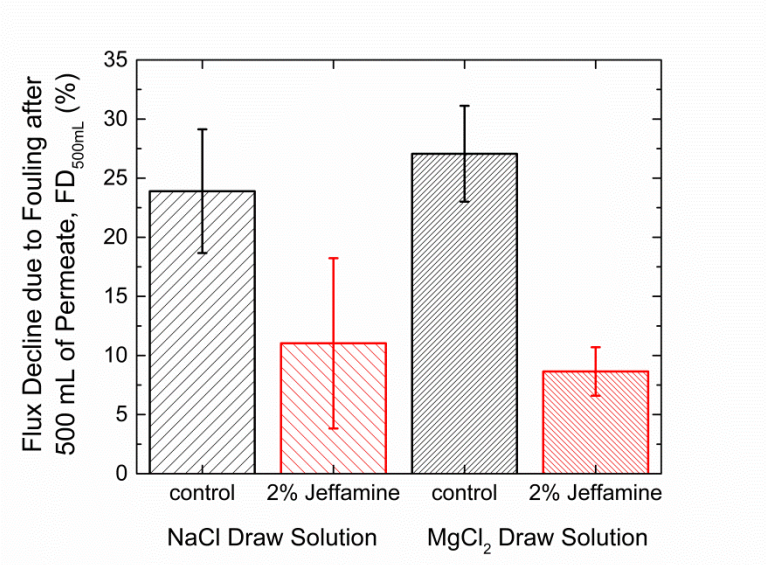

Figure 18. Comparison of permeate flux decline due to fouling after 500 mL of permeate is collected (FD_{500mL}, %) for unmodified control membranes and 2% jeffamine modified membranes. FD_{500mL} values are shown for organic fouling experiments conducted with sodium chloride (NaCl) draw solution (control n=2, modified n=3, initial baseline flux $J_{w,0}$=20.1±0.8 L m^{-2} h^{1}) and with magnesium chloride ($MgCl_2$) draw solution (control n=3, modified n=2, initial baseline flux $J_{w,0}$=17.5±1.8 L m^{-2} h^{-1}). Bars indicate the mean FD_{500mL} value, and error bars extend to one standard deviation. Foulant feed solution comprised 100 mg L^{-1} each of bovine serum albumin protein, sodium alginate, and Suwannee River natural organic matter dissolved into a synthetic secondary wastewater effluent solution (0.94 mM ammonium chloride, 0.45 mM potassium phosphate, 0.5 mM calcium chloride, 0.5 mM sodium bicarbonate, 2.0 mM NaCl, and 0.6 mM $MgSO_4$) at solution pH 7.4.

compared to 24% for the control membrane. For experiments using $MgCl_2$ draw solution, mean FD_{500mL} values for jeffamine-modified membranes and control membranes are 9% and 27%, respectively.

The improved resistance to organic fouling for the jeffamine-modified membranes indicates that the steric repulsion effect of the grafted jeffamine has effectively reduced the attachment of foulants to the membrane surfaces. The corresponding resistance to permeation from an accumulated foulant layer was reduced compared to the unmodified control membranes, and any cake-enhanced osmotic pressure associated with the fouling layer was also reduced. Thus, higher permeate water fluxes were maintained throughout the fouling experiments.

Commercial NF and RO membranes that were modified with PEG and PEG derivatives also showed reduced water flux decline compared to unmodified control membranes when exposed to model foulants, and the modified membranes were able to recover more of the initial permeate water flux after cleaning than control membranes [26-28]. Our previous work with FO membranes showed that the fouling propensity of membranes modified with PEG derivatives was reduced compared to unmodified control membranes [29, 30], as discussed further in Section 3.4.

Unmodified control membranes demonstrated a higher mean FD_{500mL} during fouling experiments conducted with $MgCl_2$ draw solution than during experiments with NaCl draw solution. Conversely, the jeffamine-modified membranes exhibit lower mean FD_{500mL} when $MgCl_2$ is used as the draw solution instead of NaCl. The different fouling trends for control and 2% jeffamine membranes are likely the result of different initial water fluxes for the experiments with NaCl and $MgCl_2$ draw solutions. Previous work has demonstrated that the initial permeate flux affects the progression of organic fouling [41], especially for BSA protein [42], which was also used in this study.

After cleaning with NaCl solution at high crossflow velocity, both control and jeffamine-modified membranes recover more than 85% of the initial permeate flux of the baseline condition. Calculated permeate water flux recoveries for the organic fouling experiments are included in Tables A1 and A2 of Appendix A. Fouling reversibility in FO is well-documented and is attributed to the relatively loose structure of the accumulated foulant layer [43]. The shapes of the flux decline curves for baseline, fouling, and recovery portions of each fouling experiment provide additional insight into the membrane fouling behavior. For the unmodified control membranes, the permeate flux decline curves for the recovery portions of the experiments (recovery curves) generally match the shapes and slopes of the flux decline curves for the fouling portions of the corresponding experiments (fouling curves). However, for the 2% jeffamine membranes, the recovery curves generally display the same slopes as the flux decline curves for the baseline portions of the corresponding experiments (baseline curves). The matching slopes of recovery and fouling curves for control membranes suggest that these membrane surfaces were not completely cleaned and restored to their pristine condition during the physical cleaning portion of the experiments, regardless of the initial flux recoveries that were demonstrated. The surfaces of fouled control membranes may remain conditioned with foulants after cleaning, such that during recovery testing, permeate fluxes decline at rates equivalent to fouling testing conditions. For the 2% jeffamine membranes, the opposite condition is indicated. Matching slopes of recovery and baseline curves suggest that organic foulants were

completely removed from the modified membrane surfaces, and in the recovery testing, the membranes behave as they did in the baseline testing prior to their exposure to foulants.

Surface adhesion forces. AFM surface adhesion forces have been strongly correlated to membrane organic fouling behavior [44], and thus, AFM measurements were collected to elucidate the mechanisms of organic fouling resistance for the modified membranes. A maximum adhesion force (F_{max}) was calculated for each AFM probe retraction event, and the corresponding distance from the membrane surface was identified. The surface interaction energy between the foulant probe and the membrane surface was approximated by dividing F_{max} by the radius of the probe colloidal particle (R_p). The quantity F_{max}/R_p is proportional to the surface interaction energy in accordance with the Derjaguin approximation [45].

Some AFM measurements exhibited no interaction energy, which was defined as one of three conditions: (i) probe retraction events where F_{max}/R_p was greater than zero, indicating repulsion from the membrane surface; (ii) probe retraction events where the absolute value of F_{max}/R_p was less than 0.05 mN m^{-1}, which is within the range of measurement noise; and (iii) probe retraction events where the absolute value of F_{max}/R_p was less than 0.10 mN m^{-1} at an associated distance greater than 300 nm, which is also within the range of the AFM measurement noise. For the unmodified control membranes, surface interaction energies were approximated for 406 measurement events, and eight "no interaction energy" events were identified. For the 2% jeffamine membranes, 281 measurement events yielded 37 "no interaction energy" events.

The mean and median values of surface interaction energies (excluding "no interaction energy" events) for the 2% jeffamine membranes are -0.32 mN m^{-1} and -0.18 mN m^{-1}, respectively. These interaction energies are not significantly different from the mean and median values of -0.32 mN m^{-1} and -0.21 mN m^{-1} for the control membranes. However, the jeffamine-modified membranes exhibit an increase in "no interaction energy" events compared to the unmodified control membranes. The observance of equivalent measured interaction energies with an increased number of "no interaction energy" events for the jeffamine-modified membrane is attributed to the non-uniform distribution of jeffamine on the modified membrane surface. When the AFM probe contacted a jeffamine-grafted area on the membrane surface, the probe experienced little attractive force or even repulsion from the surface due to the steric repulsion effect of jeffamine polymer chains. In areas of the membrane surface without grafted jeffamine, the AFM probe was essentially interacting with an unmodified membrane surface. Some "no interaction energy" events were also observed for unmodified control membranes, and these measurements may indicate less reactive areas of the membrane surface with low functional group density, as membrane surface chemistry and morphology are known to be heterogeneous [46, 47].

FO membranes modified with PEG derivatives in our previous work [29, 30] showed a decrease in the mean surface interaction energy between an AFM foulant probe and the membrane surface and also demonstrated an increase in the number of "no interaction energy" events. These membranes were modified in situ, during the membrane fabrication process. The reduced surface interaction energies for the in situ-modified membranes are a further indication that a higher density of PEG surface grafting was achieved via these in situ methods compared to this post-fabrication modification method.

Membrane Modification with Superhydrophilic Silica Nanoparticles

Optimization of modification conditions. In our previous studies,[16, 20] we showed that surface coating with superhydrophilic SiNPs imparted a significantly enhanced fouling resistance to TFC membranes. We further carried out an optimization study of modification conditions to produce the most fouling resistant membranes. Surface characteristics of the modified TFC membranes such as surface coverage of SiNPs and surface hydrophilicity were used to determine the optimal modification conditions.

To investigate the effect of the concentration of SiNP suspension on the coverage and hydrophilicity, four different concentrations for each of the two differently functionalized SiNPs (i.e., TMAC-SiNPs, and APTMS-SiNPs) were used: 0.3 wt%, 0.03 wt%, 0.003 wt%, and 0.0003 wt% at pH 7. Figure 19 shows SEM images and contact angle measurements of TMAC-SiNP modified TFC membranes (TMAC-SiNPs-TFC) at different suspension concentrations. We observed that while the highest SiNP suspension concentration led to the smallest average contact angle, the differences of contact angles for 0.3, 0.03, and 0.003 wt% were not statistically significant. In addition, SEM images show that the grafting densities of SiNPs on the membrane surface for the three concentrations were qualitatively the same. Accordingly, we determined 0.003 wt% to be the optimal concentration for TMAC-SiNPs, which results in both high SiNP coverage and surface hydrophilicity at the lowest possible SiNPs concentration. Through the same procedure, we chose 0.03 wt% as the optimal concentration for APTMS-SiNPs (Figure 20).

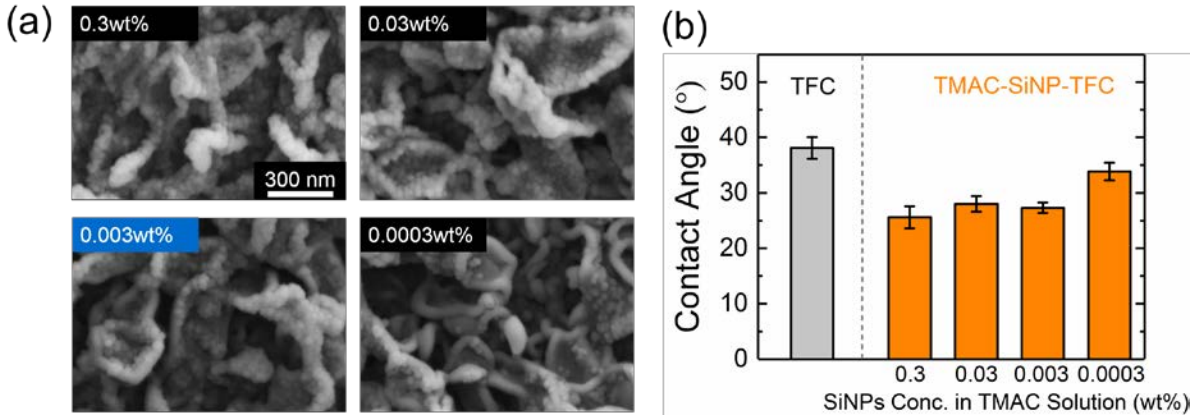

Figure 19. Effect of concentrations of TMAC functionalized silica nanoparticles (TMAC-SiNPs) suspension on membrane surface morphology and hydrophilicity after dip-coating. (a) Scanning electron microscope (SEM) images and (b) contact angles of modified membranes for different TMAC-SiNPs concentrations. The pHs of all TMAC-SiNPs suspensions were adjusted to 7.

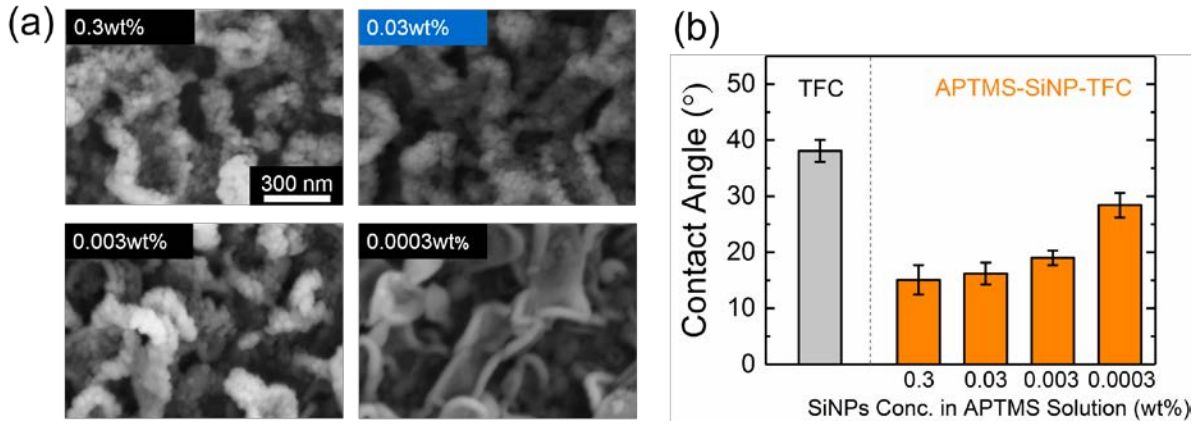

Figure 20. Effect of concentrations of APTMS functionalized silica nanoparticles (APTMS-SiNPs) suspension on membrane surface morphology and hydrophilicity after dip-coating. (a) Scanning electron microscope (SEM) images and (b) contact angles of modified membranes for different APTMS-SiNPs concentrations. The pHs of all APTMS-SiNPs suspensions were adjusted to 7.

After the optimal concentrations were determined, we investigated the effects of pH of the SiNP suspensions on the grafting density and surface hydrophilicity. Figure 21 and Figure 22 display the surface morphologies and contact angles of membranes after dip-coating in TMAC-SiNP and APTMS-SiNP suspensions, respectively, at various pHs. For both SiNP suspensions, the smallest contact angles were attained at pH 7. We attribute the most increased hydrophilicity to the strong electrostatic attraction between the membrane and the functionalized SiNPs at pH 7.

Figure 23 shows zeta potentials of the pristine TFC membrane as well as the pristine and functionalized SiNPs. TFC polyamide membranes are typically fabricated by interfacial polymerization of a monomeric polyamine with a polyfunctional acyl halide. The unreacted amine and carboxylic groups on the membrane surface dominate the membrane surface charge behavior. The surface zeta potential of the pristine membrane changes from positive to negative values with an isoelectric point at approximately pH 3.6. As the pH increases, the membrane becomes more negatively charged due to the deprotonation of the carboxyl groups as well as adsorption of anions (e.g., Cl^- and OH^-). On the other hand, the deprotonation of silanol groups renders the pristine SiNPs negatively charged at the entire pH range investigated in our measurement. As the functionalized SiNPs with APTMS or TMAC result in positive surface zeta potentials due to the amine or quaternary ammonium terminal groups, respectively, dip-coating of the membrane in the SiNPs suspension at a proper pH can lead to a dense grafting of the functionalized SiNPs.

As shown in Figure 21 and 22, the grafting densities of the SiNPs on the membrane at pH 3 are very low because the positively charged membrane surface applies repulsive forces to the positively charged SiNPs. In addition, the SiNPs with a strong positive charge can repel each other, which may further prevents the dense grafting. At pH 7, on the other hand, the membrane zeta potential becomes highly negative while the SiNPs still exhibit highly positive surface charges. This large contrast in the polarities of the membrane and the SiNPs results in the dense grafting of the SiNPs and therefore in the most hydrophilic.

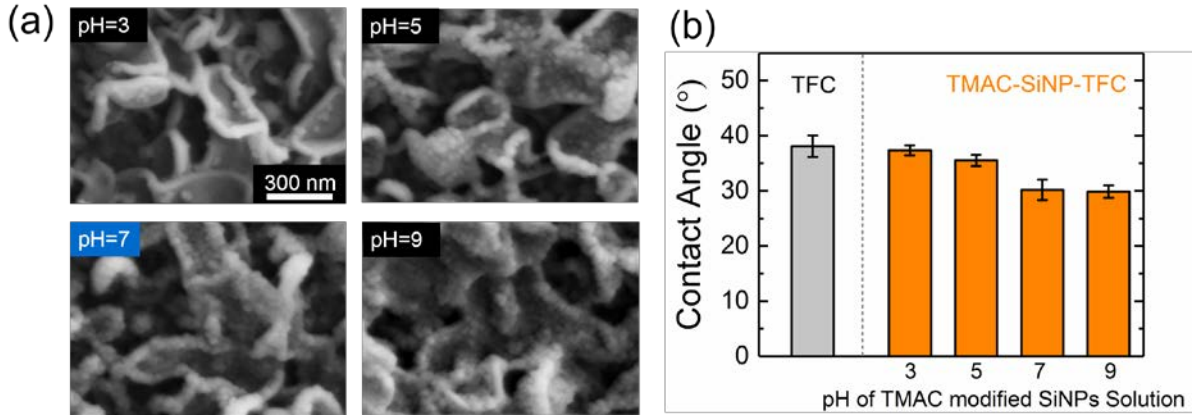

Figure 21. Effect of the pH of TMAC functionalized silica nanoparticles (TMAC-SiNPs) suspension on membrane surface morphology and hydrophilicity after dip-coating. (a) SEM images and (b) contact angles of membrane surfaces modified in TMAC-SiNPs suspensions at different pHs. Concentrations of all TMAC-SiNPs suspension were 0.003 wt%.

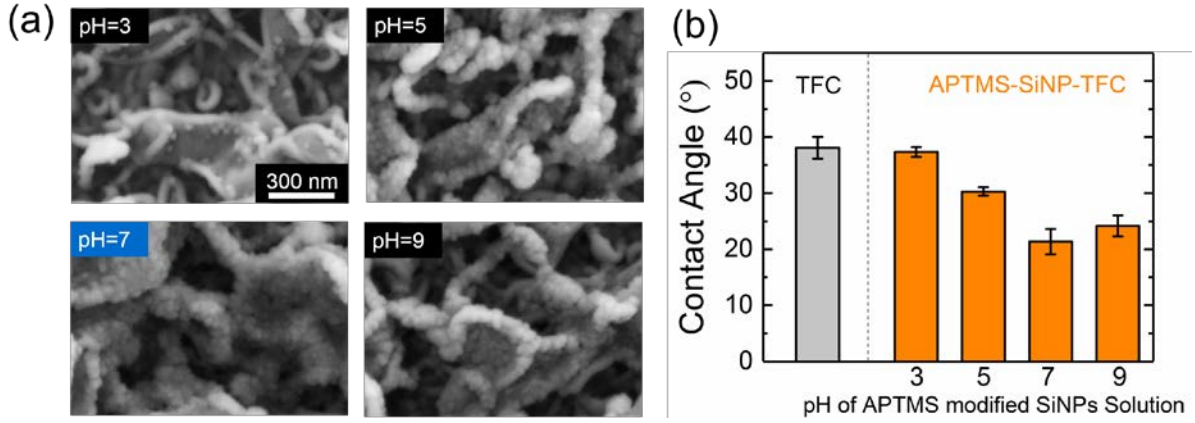

Figure 21. Effect of the pH of APTMS functionalized silica nanoparticles (APTMS-SiNPs) suspension on membrane surface morphology and hydrophilicity after dip-coating. (a) SEM images and (b) contact angles of membrane surfaces modified in APTMS-SiNPs suspensions at different pHs. Concentrations of all APTMS-SiNPs suspension were 0.03 wt%.

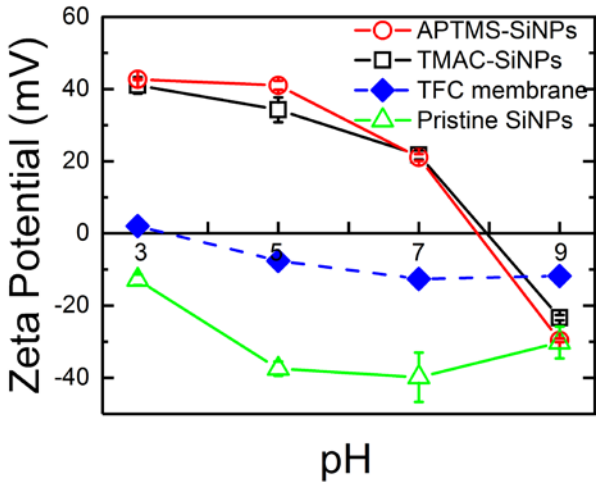

Figure 23. Zeta potentials of pristine TFC membrane, pristine and functionalized SiNPs as a function of solution pH. Membrane zeta potentials were estimated by measuring streaming potentials in the electrolyte of 1 mM KCl and 0.1 mM $KHCO_3$. Zeta potentials of SiNPs (concentration of 0.03 wt%) were obtained from electrophoretic mobility measured in the electrolyte of 1 mM NaCl. All measurements were performed at room temperature (23°C).

Membrane characteristics. We characterized intrinsic transport properties, water permeability coefficient (*A*), salt permeability coefficient (*B*), and structural parameter (*S*), of the modified membranes with the optimized SiNPs grafting (Figure 24). For both modified membranes (i.e., TMAC-SiNPs-TFC and APTMS-SiNPs-TFC membranes), nearly no noticeable changes were observed in *B* and *S*. The SiNPs modification led to a slight reduction in the water permeability coefficient (*A*), which we attribute to blockage of the surface by the grafted SiNPs. However, a student *t*-test analysis indicates that the changes in the membrane transport properties due to the

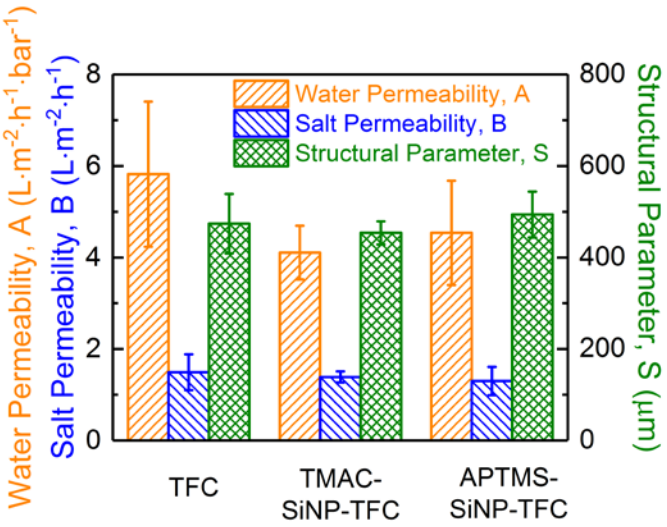

Figure 22. Transport parameters of control and modified membranes. Water permeability, *A*, salt permeability, *B* and structural parameter, *S* were measured by the FO four-step characterization method[3]. A student t-test analysis indicates that the changes in the membrane transport properties due to surface modification are not statistically significant ($p > 0.05$).

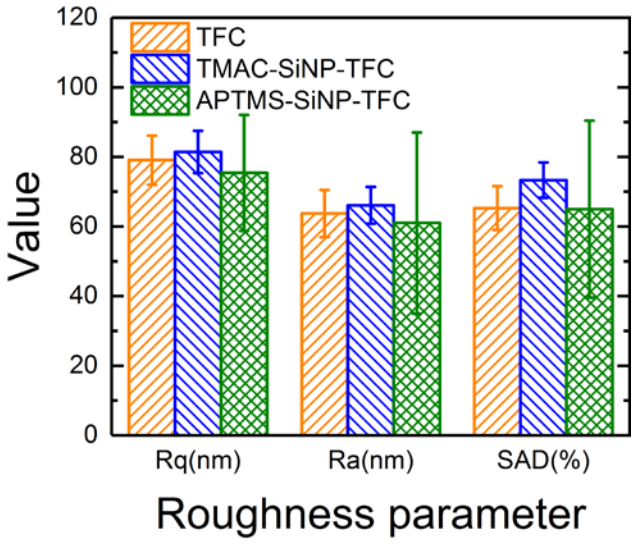

Figure 25. Surface roughness parameters of control and modified TFC membranes. R_q represents root mean square roughness, R_a is the average roughness, and SAD is a percentage surface area difference. Roughness parameters shown are the average of measurements taken from a total of 9 random spots on three separate control and modified sample surfaces. Statistical analysis (student t-test) indicates that the changes in the membrane surface roughness due to surface modification are not statistically significant ($p > 0.05$)

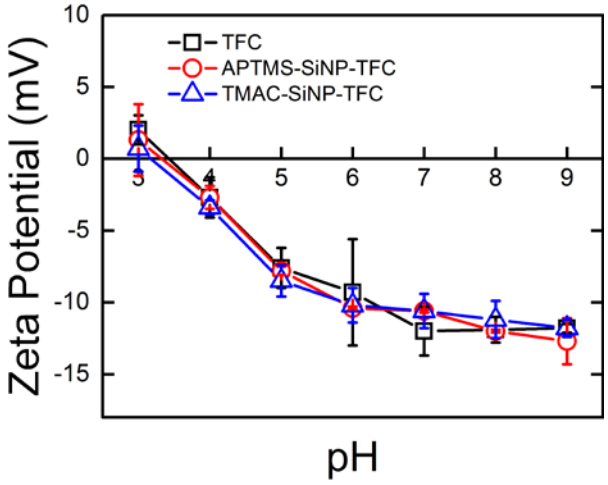

Figure 24. Zeta potentials of control and modified TFC membranes as a function of solution pH, estimated from streaming potentials measured in the electrolyte of 1 mM KCl and 0.1 mM $KHCO_3$ at room temperature (23°C).

surface modifications are not statistically significant ($p > 0.05$).

The characteristic surface roughness parameters of the membranes, i.e., root mean square roughness (R_q), average roughness (R_a), and percentage surface area difference (SAD) were measured by tapping-mode AFM (Figure 25). As shown in Figure 25, the roughness parameters did not change significantly after the grafting of SiNPs ($p > 0.05$), which is attributed to the almost even particle coverage on the ridge-and-valley membrane surface structure.

Next, we investigated the effects of SiNPs grafting on membrane surface charge. Figure 26 shows membrane zeta potential in the pH range of 3 – 9 obtained before and after the membrane modification with the SiNPs. Interestingly, the zeta potentials were not noticeably altered by the dense grafting of the functionalized SiNPs possessing positive surface charges (Figure 23). We speculate that a high density of negatively charged carboxylic groups is still freely accessible for the electrolyte and therefore dominates the charge behavior of the membranes. The possible effects of the accessible surface carboxylic groups on fouling behaviors will be discussed later.

Membrane fouling performance. To assess the fouling resistance of the SiNP-modified membranes, we performed FO dynamic fouling experiment with sodium alginate (200 mg/L), a representative polysaccharide, as a model organic foulant (Figure 27). The pristine TFC membrane showed about 28% of flux decline from the initial water flux due to fouling. On the other hand, both TMAC-SiNPs-TFC and APTMS-SiNPs-TFC membranes exhibited approximately 20% of flux decline, which we attributed to the enhanced hydrophilicity imparted by the dense grafting of superhydrophilic SiNPs.

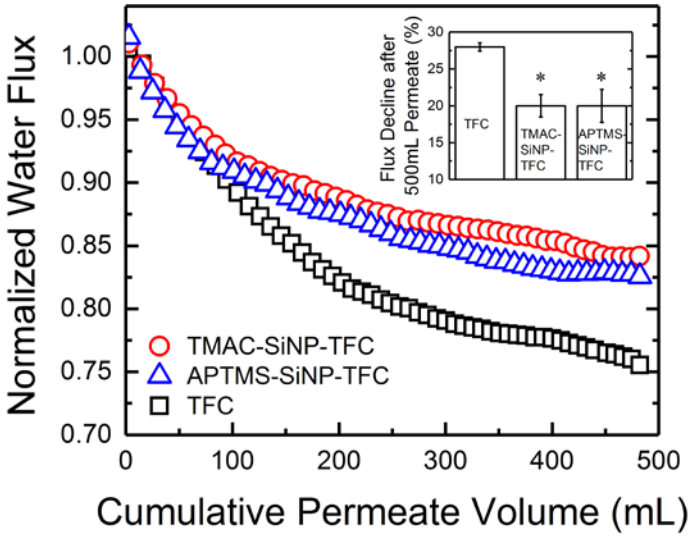

Figure 26. FO organic dynamic fouling of the control and modified TFC membranes. Fouling conditions were as follows: feed solution comprised synthetic secondary wastewater effluent (200 mM $NaHCO_3$, 930 mM NH_4Cl, 200 mM $CaCl_2$, 122 mM $MgSO_4$, 1840 mM NaCl, 90 mM KH_2PO_4) with 200 mg/L of sodium alginate with pH adjusted to 7.4, initial water flux of 20 $L \cdot m^{-2} \cdot h^{-1}$, cross-flow velocity of feed side 4.25 cm/s and draw side 9.56 cm/s, collecting a total of 500 mL volume accumulation of permeate. Temperature was maintained at 25.0 ± 0.5 °C. Water flux data were normalized by initial flux. Error bars indicate standard deviation of the normalized water flux from 4 measurements for control (TFC) and 4 for each modified membranes. Bar chart in the inset presents average flux decline after 500 mL of permeate volume were collected. "*" symbol denotes a p-value less than 0.05 in a two sided t-test, i.e., between control and each modified membranes, indicating statistically significant reduction of flux decline.

Membrane Modification with Zwitterionic Polymer Brushes

Membrane surface characteristics. SEM images and AFM roughness displaying surface morphologies of the pristine and modified membranes are shown in Figure 28. After the TFC membrane was modified by PDA (i.e., TFC-PDA), surface roughness slightly increased (Figure 28d), due to aggregates of PDA (Figure 28b). On the other hand, a smooth film was formed on the membrane surface, with a noticeably reduced surface roughness after one hour of ATRP reaction for grafting the PSBMA brush layer (i.e., TFC-PSBMA, Figure 28c, d).

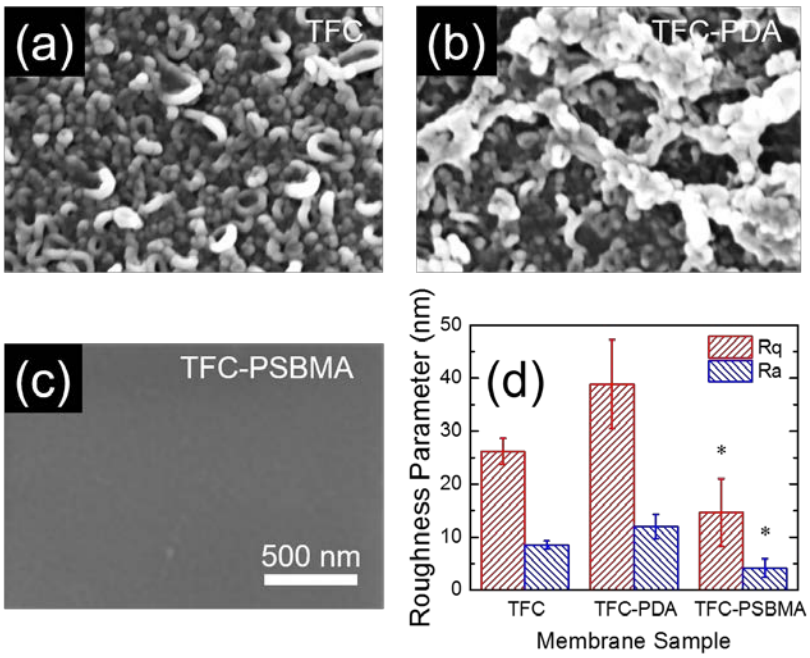

Figure 27. SEM images of the polyamide active layer of (a) pristine TFC, (b) TFC-PDA, and (c) TFC-PSBMA membranes. (d) Surface roughness determined by AFM for pristine TFC, TFC-PDA, and TFC-PSBMA membranes. The roughness parameters, i.e., mean-square value (R_q) and average roughness (R_a), were calculated from AFM images from at least six different spots on each membrane sample. Asterisks above bars indicate that the TFC-PSBMA membrane roughness parameters were significantly different ($p<0.05$) than the corresponding values of the pristine TFC membrane.

Attenuated total reflectance-Fourier transform infrared (ATR-FTIR) spectroscopy was performed to characterize the membrane surface chemistry and to further verify the successful grafting of PSBMA brushes. Figure 29a shows the spectra of the pristine and modified membranes for a wavenumber range of 1800-800 cm^{-1}, which covers the main functional groups of the modified membranes. Absorbances at 1657 and 1536 cm^{-1} correspond to (amide I) C=O stretching vibrations and (amide II) N−H band of amide group (–CONH–).[48, 49] In addition, strong peaks at 1243 cm^{-1} and 1608 cm^{-1} refer to amide III and the hydrogen–bonded carbonyl of the amide in polyamide layer, respectively. After the TFC membrane was modified with PDA (i.e., TFC-PDA), no noticeable change in the spectra was detected, likely due to the minute thickness

of the PDA and the incomplete coverage. For the PSBMA brush modified membrane (i.e., TFC-PSBMA), two additional peaks were observed at 1726 cm^{-1} and 1039 cm^{-1}, identifying the carbonyl group and sulfonate group, respectively, which are among the main functional groups of SBMA.[48]

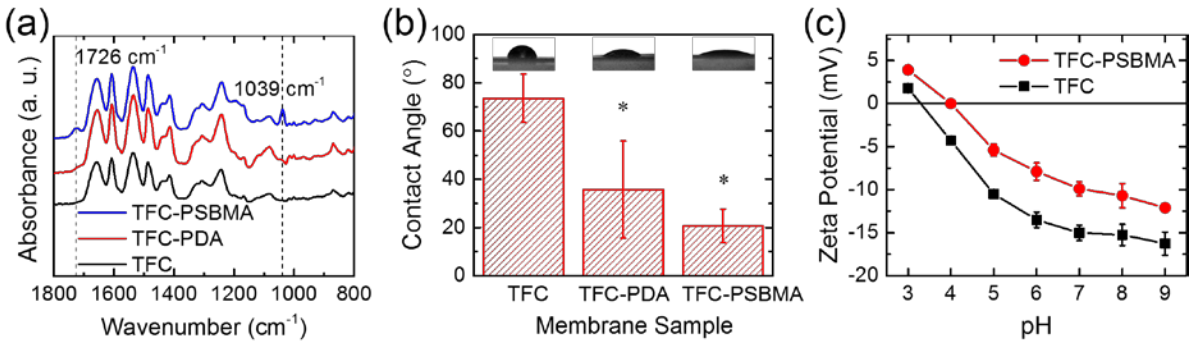

Figure 28. (a) ATR-FTIR spectra for pristine TFC, TFC-PDA, and TFC-PSBMA membranes. (b) Water contact angles for pristine TFC, TFC-PDA, and TFC-PSBMA membranes. Average values were obtained from contact angles measured on at least twelve random locations on each membrane sample. Error bars represent standard deviations. Asterisks indicate that the contact angle of the modified membrane showed a statistically significant difference compared to the pristine TFC membrane ($p<0.05$). (c) Zeta potentials of pristine TFC and TFC-PSBMA membrane surfaces as a function of solution pH. Membrane zeta potentials were estimated by measuring streaming potentials in a background electrolyte solution of 1 mM KCl and 0.1 mM $KHCO_3$. All measurements were performed at room temperature (23°C).

In order to investigate the membrane surface hydrophilicity, contact angle measurements were conducted. As shown in Figure 29b, the contact angle of TFC-PDA was significantly reduced after the deposition of PDA, showing its hydrophilic nature.[50] Modification with the PSBMA brush layer further increased the surface hydrophilicity of the membrane due to the strong hydration capacity of zwitterionic polymers.[51]

The surface charge characteristics of the pristine and modified membranes were investigated by determining the zeta potentials calculated from streaming potential measurements using the Helmoltz–Smoluchowski equation.[52] Since a typical TFC polyamide membrane is fabricated by interfacial polymerization of a monomeric polyamine with a polyfunctional acyl halide, the unreacted amine and carboxylic groups on the membrane surface dominate the membrane surface charge behavior.[53] For the investigated pH range shown in Figure 29c (i.e., pH 3 – 9), the surface zeta potential of the pristine membrane changes from positive to negative values with an isoelectric point at pH 3.3. As the pH increases, the membrane becomes more negatively charged due to the deprotonation of the carboxyl groups. Furthermore, the preferential adsorption of anions (Cl^- and OH^-) may also render the zeta potential more negative, since anions are less hydrated than cations in aqueous solutions, leading to a closer proximity to the membrane surface.[52] After the PSBMA brush was grafted, the zeta potential became less negative due to the presence of the net-zero charged zwitterionic polymer shielding the functional groups on the membrane.

The membrane transport parameters, namely water permeability coefficient, *A*, salt permeability coefficient, *B*, and structural parameter, *S*, were measured by the four-step FO characterization method.[4] As expected, the structural parameter, *S*, an intrinsic parameter relevant only to the membrane support layer, did not change after the modification of the active layer (Figure 30). It was also observed that the water permeability coefficient, *A*, of the TFC-PSBMA membrane decreased slightly while the salt permeability coefficient, *B*, increased. However, these changes were not statistically significant (based on a Student t-test) compared to the pristine TFC membrane. The precise control on the growth of the PSBMA layer via ATRP allows for further optimization of the coating thickness such that the membrane transport properties are least affected while antifouling functionality remains highly effective.

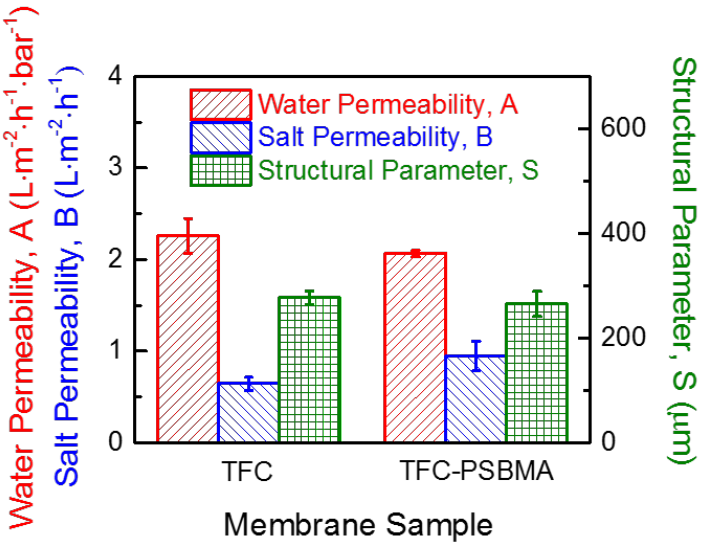

Figure 29. Transport and structural properties of pristine TFC and TFC-PSBMA membranes. Water permeability coefficient, *A*, salt permeability coefficient, *B*, and structural parameter, *S*, were measured by the four-step FO characterization method as described in the methods section.

Fouling performance. The antifouling character of the modified TFC membranes was further tested using BSA representing proteins as common foulants. Proteins are ubiquitously found in wastewater effluents and other source waters. Adsorption of proteins and other molecules on water treatment membranes not only reduces water permeability, but also leads to the formation of a conditioning layer, which may enhance microbial colonization and eventually biofouling.[54-56] Therefore, demonstration of protein fouling resistance is crucial for successful antifouling modification of TFC membranes.

We used a FITC-BSA as a model foulant to visualize membrane fouling by proteins. The fluorescence intensities of the microscopy images of the membranes after exposure to FITC-BSA qualitatively show the degrees of BSA adsorption on the surfaces (Figure 31). The bright fluorescence image of the pristine TFC membrane indicates significant adsorption of BSA. The fluorescence intensity of the TFC-PDA membrane decreased noticeably, likely due to increased hydrophilicity by deposition of PDA. In contrast, the micrograph for the TFC-PSBMA

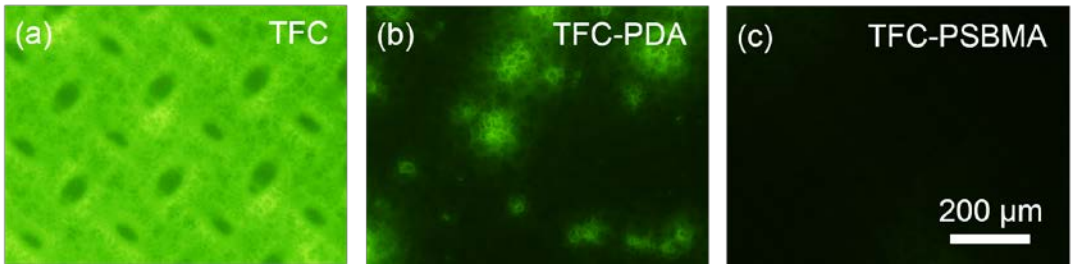

Figure 30. Epifluorescence microscopy images of pristine and modified TFC membranes following protein adhesion tests using fluorescein-conjugated BSA (BSA-FITC) in PBS. (a) Pristine TFC, (b) TFC-PDA, and (c) TFC-PSBMA membranes after three-hour exposure to BSA-FITC in PBS solution at pH 7.4.

membrane shows virtually no fluorescence, implying negligible adsorption of BSA. Such a drastic difference in BSA adsorption clearly demonstrates the excellent protein fouling resistance of the PSBMA modified membrane. We attribute this observation to the exceptionally high affinity of zwitterions to water, more than other hydrophilic materials such as polyethylene glycol (PEG).[57, 58]

The significantly increased hydrophilicity of the TFC-PSBMA membrane (Figure 29b) implies that the grafting of zwitterionic polymer brushes may enhance fouling resistance. We employed chemical force microscopy to assess the organic fouling propensity of the modified membranes, with a carboxylated latex particle attached to an AFM cantilever serving as a model organic foulant. Most organic foulants (e.g., natural organic matter, polysaccharides, and proteins) possess carboxylic groups, which aggravate fouling by complex formation with carboxylic groups on polyamide-based TFC membrane surfaces in the presence of calcium ions.[59-61] Therefore, interaction forces between the membrane surface and the carboxylated particle can provide a quantitative measure of membrane fouling propensity.

Figure 32 presents the frequency distributions of adhesion forces (normalized to the latex particle radius) for the pristine and modified membranes in aqueous solution containing calcium ions. For the pristine TFC membrane, the average interaction force was -0.92 ± 0.6 mN/m, exhibiting adhesive forces (i.e., negative values), with a very small fraction of non-adhesive events (indicated as “NO” in Figure 32a). The significant adhesive forces observed with the control TFC membrane are mainly attributed to intermolecular bridging mediated by calcium ions.[44]

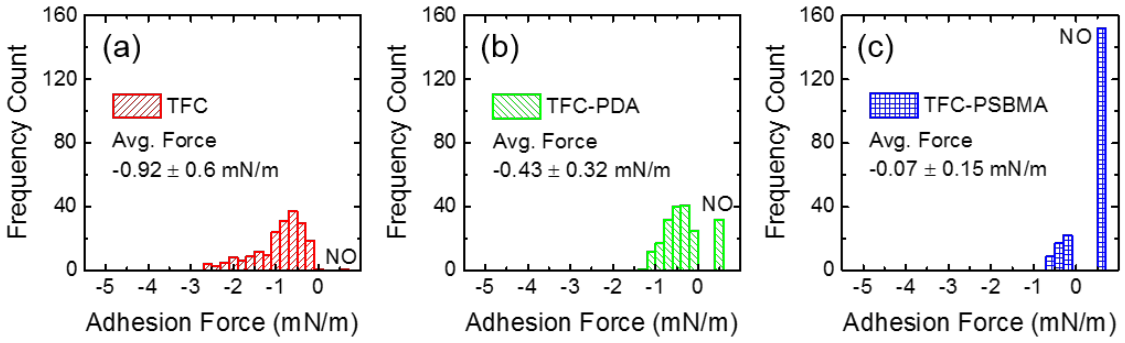

Figure 31. Distributions of adhesion forces between a model foulant (carboxylatetd latex particle) and (a) control TFC, (b) TFC-PDA, and (c) TFC-PSBMA membranes measured by AFM. The "NO" label (at the positive force range) stands for measurements where no adhesion force was observed. The test solution for the measurements comprised 50 mM NaCl and 0.5 mM $CaCl_2$ at room temperature (23 °C). Five locations were randomly selected for each membrane sample, and at least 40 measurements were taken at each location. Average values of the adhesion forces are also presented.

After the membrane was modified by PDA (i.e., TFC-PDA membrane), the adhesion forces were significantly reduced to -0.43 ± 0.32 mN/m, with an increased frequency of non-adhesive events (indicated as "NO" in Figure 32b). Because PDA partially covers the carboxylic groups on the membrane surface, calcium-ion bridging is expected to be less prominent, which would result in a reduced adhesion force between the TFC-PDA membrane and foulants.

The TFC membrane grafted with zwitterionic polymers (TFC-PSBMA) showed a much narrower distribution of adhesion forces centering at markedly lower value, -0.07 ± 0.15 mN/m, representing a 92% reduction in average adhesion force compared to the pristine membrane. The apparent PSBMA film, observed in SEM images (Figure 28c), shields the surface carboxylic groups and thus effectively prevents calcium-ion induced fouling. Swelling of the PSBMA brush layer can also contribute to a further reduction of the foulant-membrane adhesion force by increasing the distance between the solid-water interface and the membrane surface.[51]

The results of the chemical force microscopy and static fouling experiments strongly suggest that zwitterionic PSBMA brushes impart TFC membranes with excellent organic fouling resistance. To further assess the antifouling property of the modified membranes in a more realistic setting and for long-term applications, FO fouling experiments with organic foulants were conducted for both pristine and zwitterion-modified membranes.

Figure 33 displays water flux behavior (corrected for draw solution dilution effects) for the pristine TFC and TFC-PSBMA membranes. The data represent the average of three independent fouling experiments. Our results demonstrate a significant fouling resistance for the TFC-PSBMA membrane compared to the control TFC membrane. After 500 mL of permeate volume, the pristine TFC membrane showed a 25% decline in water flux, while the TFC-PSBMA membrane exhibited a remarkably lower flux decline of 15%. Again, the dynamic fouling experiments clearly demonstrate the excellent antifouling functionality of the zwitterionic polymer brushes, highlighting the promise of our surface modification technique for membrane fouling mitigation.

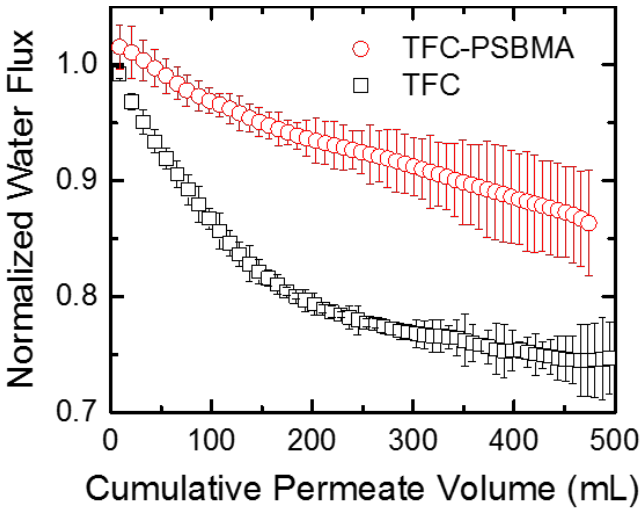

Figure 32. Normalized water flux due to fouling as a function of cumulative permeate volume of the pristine TFC and TFC-PSBMA membranes during FO dynamic fouling tests. Fouling conditions were as follows: composition of the feed solution simulated secondary wastewater effluent (0.5 mM NaHCO3, 0.93 mM NH4Cl, 0.5 mM CaCl2, 0.61 mM MgSO4, 9.2 mM NaCl, and 0.45 mM KH2PO4) with a mixture of three organic foulants: 100 mg/L of sodium alginate, 100 mg/L BSA, and 100 mg/L SRNOM. Solution pH was adjusted to 7.4 and initial water flux was 20 L m-2 h,-1 adjusted for each experiment by an NaCl draw solution (concentration ranged from 0.7 to 0.9 M). Cross-flow velocity of feed and draw solutions in the membrane cell were 4.25 and 9.56 cm/s, respectively. Temperature was maintained at 25.0 ± 0.5 °C. Fouling experiments were performed until 500 mL cumulative volume of permeate was collected, lasting ~17.4 hours for pristine TFC and ~16 hours for TFC-PSBMA membranes.

Optimal Post-fabrication Modification for Development of TFC Membranes with the Highest Fouling Resistance

TFC membranes modified by the three different post-fabrication techniques using jeffamine, SiNPs and zwitterionic polymer brush exhibited enhanced fouling resistances compared to pristine TFC membranes. Since TFC membranes used in OsMBR are required to have a high fouling resistance against the constantly exposed foulants in a long operation time period, we sought the most promising method that can impart the highest fouling resistance to the TFC membrane without significantly affecting membrane transport properties. We performed a comparative study based on assessment of the fouling resistance against common foulants in realistic settings.

We note that jeffamine-based post-fabrication modification may not be an ideal technique for the membrane modification. As discussed in Section “Membrane Modification Using jeffamine” and Figure 17, the non-uniform distribution of Rhodamine dye-tagged jeffamine molecules suggests that anchoring of Jeffeamine on the membrane surface by EDC-NHS chemistry does not lead to a dense grafting of the jeffamine. In addition, the poor coverage of jeffamine resulted in the increased surface roughness, which can aggravate organic fouling. Therefore, we excluded the jeffamine-based post-fabrication technique for the comparative study, and only compared the fouling resistances of TFC membranes modified by SiNPs-based and zwitterionic polymer-based techniques.

Comparison of SiNPs and Zwitterionic Polymers Related Post Modification

Membrane surface characteristics. The surface morphology of the modified membranes was first examined by SEM and AFM (Figure 34a, b). The pristine TFC membrane surface exhibited a typical ridge-and-valley morphology, originated from interfacial polymerization reaction to form polyamide [62]. After dip-coating with SiNPs, the membrane surface was covered by a dense layer of nanoparticles (Figure 34a). On the other hand, no distinct visual change was observed after a one hour modification of the membrane with PSBMA brushes. This observation indicates that a very thin PSBMA brush layer was formed after the one hour ATRP reaction

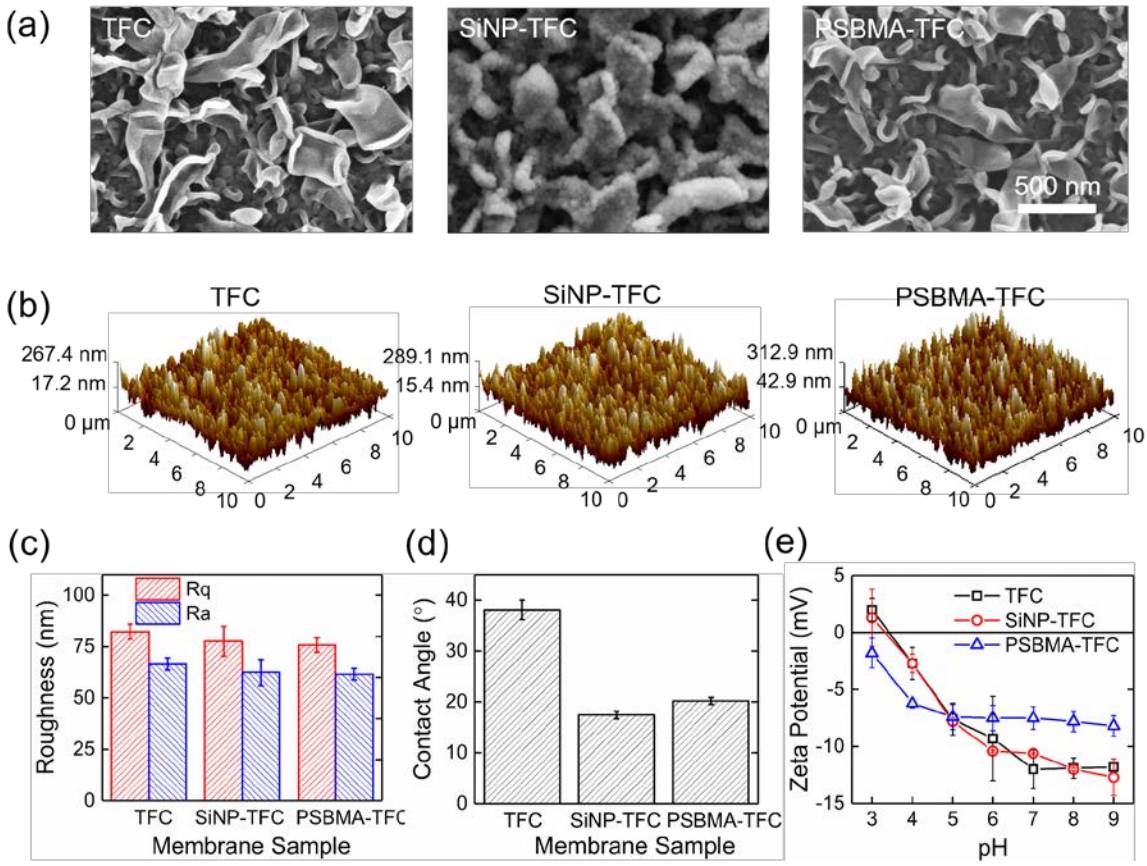

Figure 33. Surface characteristics of pristine and modified TFC membranes. (a) SEM images of the active layer of pristine TFC, SiNP-TFC and PSBMA-TFC membranes. (b) AFM 3D images, and (c) Roughness parameters of pristine TFC, SiNP-TFC, and PSBMA-TFC membranes. Parameters Rq and Ra represent root mean squared roughness and average roughness, respectively, which were collected from six different samples with an area of 10 μm × 10 μm scanning size for each membrane. (d) Water contact angles of pristine TFC, SiNP-TFC, and PSBMA-TFC membranes. The average values were obtained from contact angle measurements performed on at least twelve random locations on each membrane sample. (e) Zeta potentials of pristine TFC, SiNP-TFC, and PSBMA-TFC membrane surfaces at pH ranged from 3-9. All measurements were performed at room temperature (23°C).

(Figure 34a).

The morphological change due to the modification was quantified using surface roughness parameters estimated by AFM (Figure 34c). After modification with either SiNPs or PSBMA brushes, the roughness parameters were marginally reduced from those of the pristine membrane. For example, the root mean squared roughness (R_q) of membrane surface only decreased by ~ 7% after the membranes were grafted with SiNPs or PSBMA brushes. This small change in roughness corroborates with the conformal and dense coating of SiNPs and the thin PSBMA brush layer on the membrane surface (Figure 34a, b). In our study, we used a one hour ATRP reaction for grafting of the PSBMA brush, resulting in surface roughness parameters comparable to those of the membrane modified with SiNPs. Since higher surface roughness may lead to more severe fouling [31, 63], this allows us to exclude roughness effects when comparing fouling behaviors of the membranes modified with two different materials.

Next, we evaluated surface hydrophilicity of the modified membranes by measuring water contact angles (Figure 34d). While the pristine TFC membrane is relatively hydrophilic (contact angle of 38° ± 1.9°), the modification with SiNPs and PSBMA brushes further increased the hydrophilicity to almost the same extent, with contact angles of 17° ± 0.7° and 20° ± 0.7°, respectively. Since the surface roughness was identical for both modified membranes, the observed surface hydrophilicity increase should reflect the surface chemistry of the coating materials (i.e., SiNPs and PSBMA). Although the surface functional groups of the two materials are different, the comparable contact angles rule out the impact of surface hydrophilicity on the fouling propensity of the two differently modified membranes.

We also obtained surface zeta potentials of the membranes to investigate surface charge characteristics (Figure 34e). The polyamide active layer of TFC membrane is formed by the reaction between polyfunctional amine and polyfunctional acyl halide monomers, which results in a high surface density of carboxylic groups. As a result, more negative zeta potentials were obtained as pH increased due to the deprotonation of the carboxylic groups [52]. Interestingly, the zeta potentials were not noticeably altered by the dense grafting of the functionalized SiNPs, which possess positive surface charges imparted by APTMS, we suspect that a high density of negatively charged carboxylic groups is still freely accessible to the electrolyte and therefore dominates the charge behavior of the membrane. In contrast, the zeta potentials were significantly reduced after the grafting of PSBMA brushes because the net zero-charged, zwitterionic PSBMA brush layer covers the membrane surface [64].

The intrinsic transport parameters for the pristine and the modified membranes, namely water permeability coefficient (*A*), salt permeability coefficient (*B*) and structural parameter (*S*), were determined in a cross-flow FO unit using the four-step method (Figure 35) [4]. As expected, the structural parameter, which reflects the property of the membrane support layer, was not affected by the active layer modification with either SiNPs or zwitterionic polymer brushes. The changes in water permeability and salt permeability after membrane modifications were also not statistically significant, probably due to the small thickness of the SiNPs or PSBMA coating.

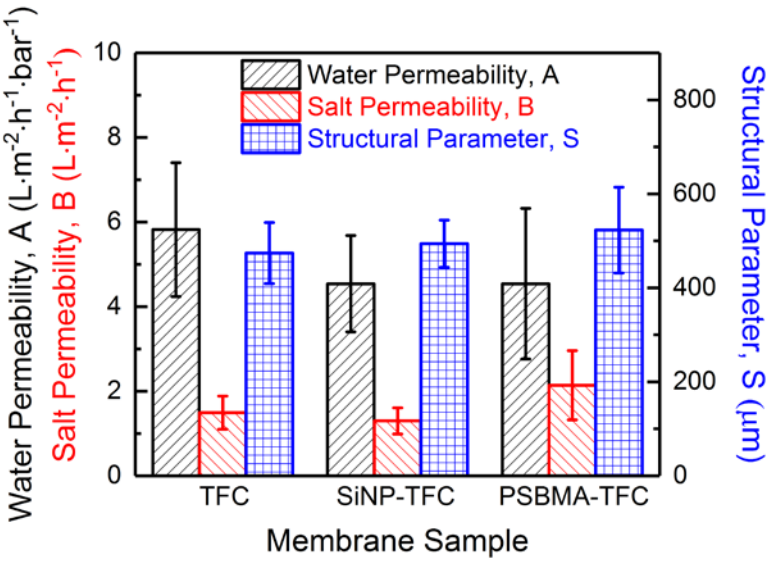

Figure 34. Transport parameters, including water permeability coefficient (*A*), salt permeability coefficient (*B*), and structural parameter (*S*) of pristine TFC, SiNP-TFC, and PSBMA-TFC membranes. These parameters were measured by the FO four-step characterization method [4].

Fouling performance. Static protein adsorption and bacteria adhesion assays were carried out to evaluate fouling resistance of the modified membranes. Proteins are ubiquitously found in wastewater effluents and other water sources. Adsorption of proteins not only reduces water permeability of membranes [65], but also leads to the formation of a conditioning layer conducive to the growth of bacteria, which accelerates biofouling [66]. Therefore, demonstration of protein fouling resistance is essential for proving the antifouling performance of the modified membranes.

Protein adsorption on the modified membranes was assessed from florescence images of the membrane surface after exposure to the FITC-BSA solution for three hours. Figure 36 displays representative fluorescence images of pristine TFC and modified membranes as well as normalized fluorescence intensities. Florescence intensity of the images qualitatively shows the density of the adsorbed proteins on the membrane surface. The bright fluorescence (i.e., high florescence intensity) of the pristine membrane indicates a significant adsorption of the BSA. The SiNPs-TFC membrane showed an 8% increase in fluorescence intensity compared to the pristine membrane, suggesting a poor fouling resistance against BSA. Despite the superior hydrophilicity imparted by SiNPs, the electrostatic interaction between the negatively charged BSA surface and the positively charged, functionalized SiNPs still seems to be the prevailing fouling mechanism. This result implies that the high surface hydrophilicity may not be sufficient to prevent fouling induced by electrostatic interactions. Similarly, fouling of pristine silica particles by positively charged proteins has been also reported [67].

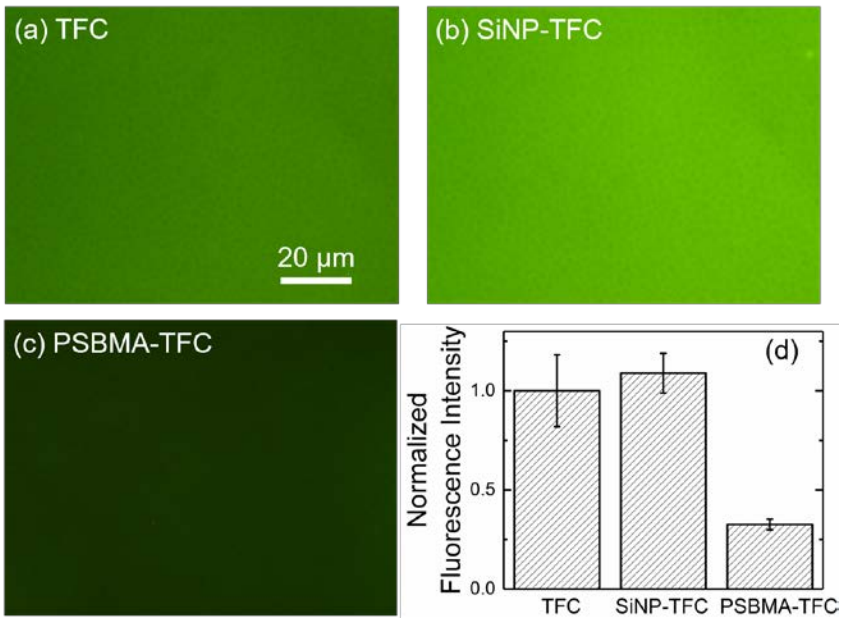

Figure 35. Epifluorescence microscopy images and relevant fluorescence intensity of pristine and modified TFC membranes after protein adhesion tests using fluorescein-labeled BSA (FITC-BSA, 0.05 mg/mL) in PBS. (a) Pristine TFC, (b) SiNP-TFC, and (c) PSBMA-TFC membranes after exposure to FITC-BSA solution at pH 7.4 for three hours. (d) Average fluorescence intensity normalized by that of the pristine TFC membrane. Ten images for each membrane sample were used to obtain average values.

In contrast, the PSBMA-TFC membrane exhibited a significantly reduced BSA adsorption with a 68% decreased fluorescence intensity from that of the pristine membrane. The equally distributed opposite charge units in zwitterionic polymers lead to the formation of a tight hydration layer [68, 69], thereby hindering protein adsorption. Additionally, the PSBMA layer with net-zero charge reduces electrostatic interactions between the membrane and charged foulants.

Fouling resistance against microorganisms is also critical for antifouling TFC membranes since proliferation of adsorbed microorganisms eventually leads to biofouling [70]. We investigated the fouling resistance of the modified membranes against microorganisms using adsorption tests with *E. coli* as the model bacteria. For both of the modified membranes, we observed close to no dead cells, which is expected as neither SiNPs nor zwitterions are bactericidal (data not shown).

After exposure to bacteria suspension and subsequent rinsing, a significant number of live *E.coli* (i.e., $1.44 \pm 0.30 \times 10^5$ cells / cm^2) remained on the pristine TFC membrane (Figure 37). The coating of SiNPs aggravated the fouling by *E. coli*, exhibiting an approximately 45% increase in the number of adsorbed bacteria on the SiNPs-TFC membrane compared to the pristine membrane. This result is consistent with the significant BSA adsorption on the SiNPs-TFC membrane (Figure 36), showing the dominant effect of the electrostatic attraction between the positively charged SiNPs-TFC membrane and the negatively charged bacteria surface [55]. In contrast, the coating of PSBMA brushes on the TFC membrane drastically increased the fouling resistance against bacteria, exhibiting a 96% reduction of the number of attached *E. coli*

compared to the pristine TFC membrane. This excellent antifouling property imparted by zwitterionic polymer brushes is consistent with the negligible protein adsorption (Figure 37).

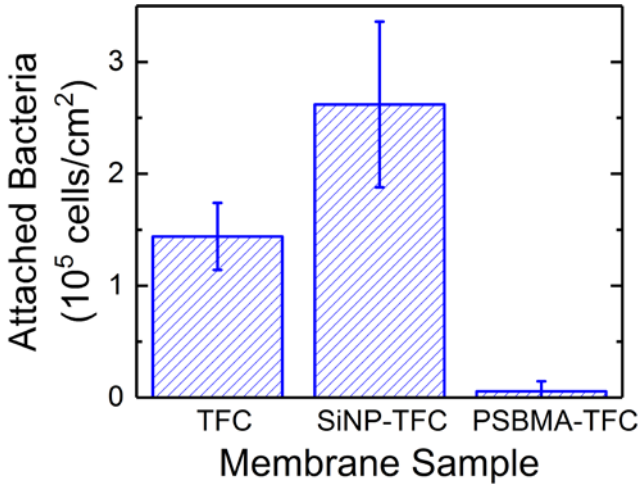

Figure 36. Numbers of attached, live bacteria (*E. coli*) per membrane surface area for pristine and modified membranes after exposure to bacteria suspension for three hours. Cell counts were obtained from at least 20 images per membrane sample and the images were acquired with an epifluorescence microscope after the membrane were stained with SYTO® 9 (green) dye specific for live cells.

In order to compare the antifouling property of the modified membranes in more realistic settings, we performed fouling experiments in FO mode with sodium alginate as a model organic foulant. Water flux data was obtained until 500 mL cumulative permeate volume was collected to evaluate the fouling behaviors of the pristine and modified membranes. As shown in Figure 38, a significant water flux decline (~ 24 %) was observed for the pristine membrane after 500 mL of permeate volume was collected. The SiNPs-TFC membrane exhibited a moderately reduced water flux decline (~ 17 %), showing a certain degree of fouling resistance that is most likely due to the increased surface hydrophilicity. The flux decline of the PSBMA-TFC membrane was further reduced to 10 %, proving the excellent antifouling property of the zwitterionic polymer brush layer.

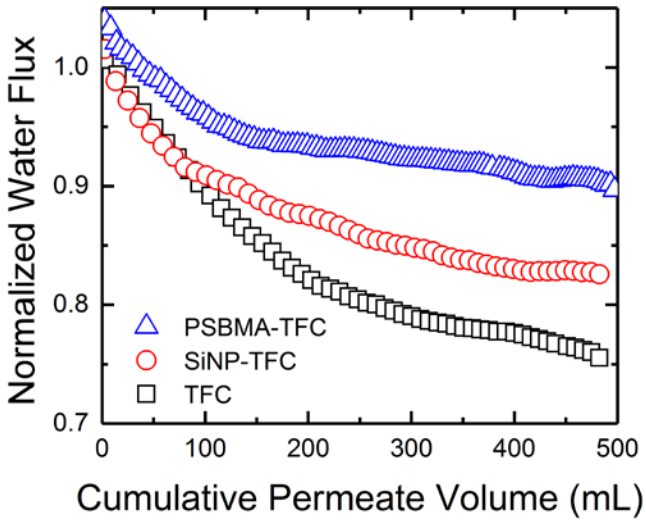

Figure 37. Normalized water flux due to fouling (excluded draw solution dilution effect) as a function of cumulative permeate volume for the pristine TFC, modified SiNP-TFC and PSBMA-TFC membranes from dynamic fouling experiments using cross-flow FO mode. Fouling conditions were as follows: the ionic composition of the feed solution simulated secondary wastewater effluent (0.93 mM NH_4Cl, 0.5 mM $NaHCO_3$, 0.61 mM $MgSO_4$, 0.5 mM $CaCl_2$, 9.2 mM NaCl, and 0.45 mM KH_2PO_4) with 200 mg/L of sodium alginate as a model organic foulant. The pH of the feed solution was adjusted to 7.4. The initial water flux was 20 $L \cdot m^{-2} \cdot h^{-1}$ adjusted by an NaCl draw solution (concentration ranged from 0.64 to 0.73 M). Cross-flow velocities of feed and draw sides were 4.25 cm/s and 9.56 cm/s, respectively. Temperature was maintained at 25.0 ± 0.5 °C. Fouling experiments performed to attain 500 mL cumulative volume lasted ~16.5 hours for pristine TFC, ~15.9 hours for SiNPs-TFC, and ~15.6 hours for TFC-PSBMA membranes. The displayed traces of water flux were averaged values of triplicate measurements for each membrane.

Despite the same degree of enhancement of surface hydrophilicity as a result of SiNPs coating or PSBMA brush grafting, the PSBMA-TFC membrane exhibits remarkably improved fouling resistance than the SiNPs-TFC membrane in static adsorption tests with proteins and bacteria as well as in dynamic FO fouling experiments. We performed chemical force microscopy to assess fouling propensity of the modified membranes with a carboxylated latex microparticle attached to an AFM cantilever, serving as a general organic foulant [42, 71]. Most organic foulants possess carboxylic groups, which aggravate organic fouling of polyamide TFC membranes via calcium-ion induced complexation [61]. Therefore, the measurement of interaction forces between the membranes and foulants in the solution with and without calcium ions allows us to identify the specific interfacial interaction that dominates fouling mechanisms. We used a PBS buffer and a solution of NaCl and $CaCl_2$ as testing saline solutions, the former to exclude and the latter to include the effects of calcium-ion induced fouling.

Figure 39(a) presents the frequency distributions of adhesion forces (normalized by the latex microparticle radius) for the pristine and modified TFC membranes measured in the PBS buffer. The pristine TFC membrane exhibited a high portion of non-adhesion events (48%, shown in "NO" column) with the average intermolecular force centered at -0.09 ± 0.21 mN/m (negative values represent adhesion forces). After the membrane was modified with SiNPs, the average adhesion force was increased by approximately 36% (i.e., -0.14 ± 0.23 mN/m) while the PSBMA-TFC membrane showed the lowest adhesion forces (i.e., -0.07 ± 0.14 mN/m). These

results are consistent with the adsorption tests using BSA and *E. coli* (Figure 36 and 37), suggesting that despite the enhanced hydrophilicity, the electrostatic interactions between the negatively charged surface of the foulants and the positively charged surface of the functionalized SiNPs (Figure 23) can aggravate fouling even in the absence of calcium ions. On the other hand, the lowest level of adhesion forces of the PSBMA-TFC membrane suggests that the zero-charged zwitterionic PSBMA brush layer suppresses the electrostatic interactions and therefore decreases the fouling propensity.

The distribution of interaction forces acquired in the solution of 50 mM NaCl and 0.5 mM $CaCl_2$ is shown in Figure 7(b). The pristine TFC membrane exhibits significantly larger adhesion forces (i.e., -0.31 ± 0.20 mN/m) compared to those in the PBS solution, which clearly shows that calcium ions aggravate fouling via complexation of carboxylic groups. After the modification with either SiNPs or zwitterionic polymer brushes, the average adhesion forces for both membranes (i.e., SiNPs-TFC and PSBMA-TFC membranes) decreased significantly, and to the same extent, showing a 61% reduction from the pristine membrane. This is likely because the coating layer of SiNPs or zwitterionic polymer brushes physically interferes with the complexation between the carboxylic groups on the membrane and on the latex microparticle.

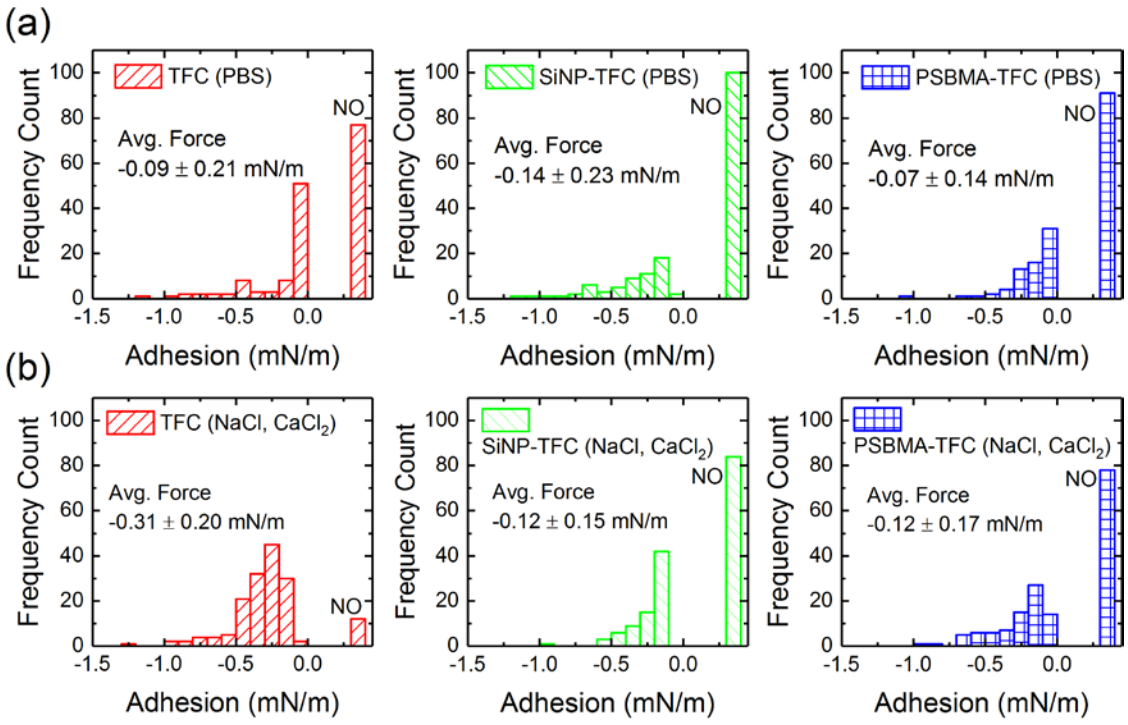

Figure 38. Frequency distributions of adhesion forces (normalized by the latex microparticle radius) between a carboxylated latex particle attached on the AFM probe and membranes (pristine TFC, SiNP-TFC, and PSBMA-TFC) measured in (a) PBS solution, (b) 50 mM NaCl and 0.5 mM $CaCl_2$ solution. The columns labeled "NO" at positive force values indicate measurements where no adhesion force was observed.

Interestingly, the PSBMA-TFC membrane exhibited a noticeably smaller water flux decline than the SiNPs-TFC membrane in the FO fouling experiment with the feed containing calcium ions (Figure 38). Although the same degree of the reduced fouling propensity was observed for both

membranes in the adhesion force measurements by AFM (Figure 39b), we suspect that small foulants with low molecular weights (e.g., alginate) may still interact with the underlying surface functional groups of the TFC membrane despite the surface is covered by SiNPs. As previously discussed, the surface zeta potentials of the modified membrane with APTMS-functionalized SiNPs (i.e., SiNs-TFC membrane) were almost identical to those of the pristine membrane (Figure 34e), suggesting that the surface carboxylic groups can still freely come into contact with feed solutions and foulants even after being coated with SiNPs. Moreover, the membrane surface is continuously exposed to more highly concentrated foulants than those in the bulk owing to the advection of foulants toward the membrane surface by the permeate water flux and rejection by the active layer. Hence, while the enhanced surface hydrophilicity contributes to increasing fouling resistance, calcium-ion induced complexation may aggravate organic fouling. It is also worth mentioning that the electrostatic attraction between the positively charged SiNPs and negatively charged foulants (i.e., alginate) should be more prominent in the FO experiment than in the static adsorption test and the chemical force microscopy, due to the ionic strength of the FO feed solution (i.e., ~ 10 mM) being lower than those of testing solutions used in the adsorption tests and adhesion force measurements (i.e., ~ 50 – 150 mM).

On the other hand, the grafting of PSBMA brushes effectively shields the underlying carboxylic groups on the membrane surface from the feed solutions, evidenced by the less negative surface charge of the PSBMA-TFC membrane than that of the pristine membrane (Figure 34e). The brush layer decreases the exposure of carboxylic groups to foulants and thereby prevents calcium ion-induced organic fouling. Moreover, the swelling of the zwitterionic polymer may provide an effective physical and chemical barrier against the adsorption of foulants.

Demonstration of Fouling Resistance of Zwitterionic Polymer-Modified Membrane in an OsMBR Using Real Wastewater

We conducted a collaborative work with Prof. Amy Childress group at the University of Southern California to test the fouling resistance of thin-film composite (TFC) membranes

Table 1. Characteristics of Return Activated Sludge used in the OsMBR experiments.

Property	RAS Sample 1	RAS Sample 2
Chemical Oxygen Demand (COD) (mg/L)	2498	1851
Volatile Suspended Solids (VSS) (g/L)	3.66	2.57
Total Suspended Solids (TSS) (g/L)	7.89	5.59
Ionic Conductivity (mS/cm)	1.72	1.72

modified with a zwitterionic polymer brush layer (TFC-PSBMA) in an OsMBR. A 300 L of return activated sludge (RAS) was obtained from Hyperion wastewater treatment plant in Los Angeles, California. The RAS was introduced into the bioreactor as a feed solution and water was reclaimed from the RAS via forward osmosis with the modified membranes. The solution properties of two batches of RAS used in our experiments are shown in Table 1.

We prepared TFC-PSBMA membranes, which were modified via deposition of polydopamine (PDA) for 15 minutes followed by 1 hour ATRP reaction to graft PSBMA polymer brushes. Figure 40 shows the transport properties (i.e., A, B, and S values) of the modified membranes determined by 4-step method in a forward osmosis mode [4]. We observed that the water permeability (A) of the modified membrane was decreased approximately 30% from that of pristine membranes. On the other hand, changes in the salt permeability (B) and the structural parameter due to the modification were not statistically significant based on the student t-test. Before the fouling test, NaCl solutions with two different concentrations were used as feed and draw solutions to achieve a stable initial water flux. The NaCl concentration in the feed solution was set to have the same conductivity of the RAS (i.e., 1.73 mS/cm). The draw solution concentration was then adjusted to reach the water flux of approximately 10 $L \cdot m^{-2} \cdot h^{-1}$. The cross-flow velocity of the draw and feed solutions was set to be 20 cm/s, and temperature was maintained at 30.0 ± 1.0 °C. After 1 hour, the feed solution was replaced by the flow from an aerated bioreactor that contained 15 L of RAS from Hyperion wastewater treatment plant, which initiated fouling experiments.

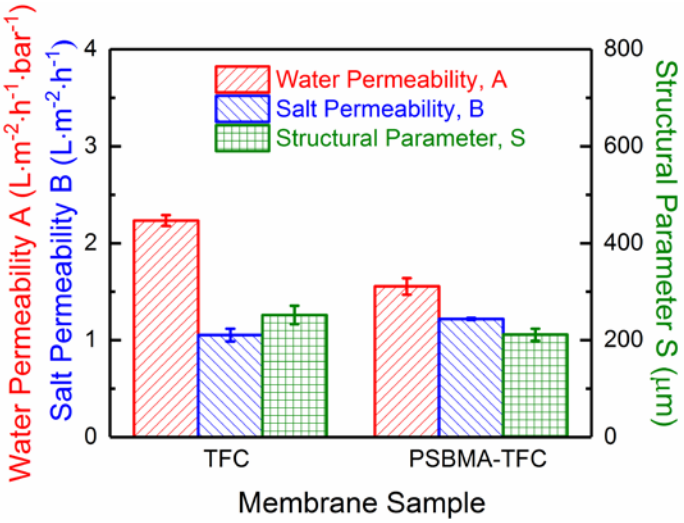

Figure 39. Transport and structural properties of pristine TFC and TFC-PSBMA membranes used in OsMBR experiments. Water permeability coefficient, *A*, salt permeability coefficient, *B*, and structural parameter, *S*, were measured by the four-step FO characterization method as described in the methods section.

Figure 41 shows time traces of water flux for pristine TFC and TFC-PSBMA membranes until 450 mL of cumulative permeate volumes were reached (Figure 41). For RAS Sample 1 with the

higher total suspended solids (TSS), the pristine TFC and TFC-PSBMA membranes exhibited 50.8% and 41.8% water flux decline, respectively, demonstrating the improved fouling resistance of the zwitterionic polymer-modified membrane. For RAS Sample 2 with the lower TSS, the PSBMA-modified membrane again exhibited a considerably reduced flux decline (26.3%) compared to that of the pristine membrane (37.1%). These significantly delayed fouling behaviors clearly demonstrate the promise of the zwitterionic polymer modified TFC membranes for efficient and robust OsMBRs.

Despite the improved fouling resistance of TFC-PSBMA membranes, we note that fouling is inevitable. Due to the advection of foulants toward the membrane by the permeate flow and foulant rejection by the active layer, the membrane surface is continuously exposed to foulant concentration higher than the bulk. Once foulants adsorb to the membrane surface, the PSBMA brush layer is not effective and the dominant interaction occurs between the newly approaching foulants and the already deposited foulants.

We emphasize the importance of further optimization of the grafting density of PSBMA brushes and size of the polymer chain in order to maximize the utility of the developed technique for large-scale applications. Employing a longer duration of PDA deposition is anticipated to increase the surface density of initiators, leading to a high grafting density of the PSBMA brushes. In addition, the size of PSBMA brushes can be increased via employing a longer duration of ATRP reaction. Optimization studies to produce a sufficiently thick layer of dense brushes while maintaining the membrane permeability and selectivity will be a key to successful implementation of the developed strategy for large-scale application of antifouling FO membranes.

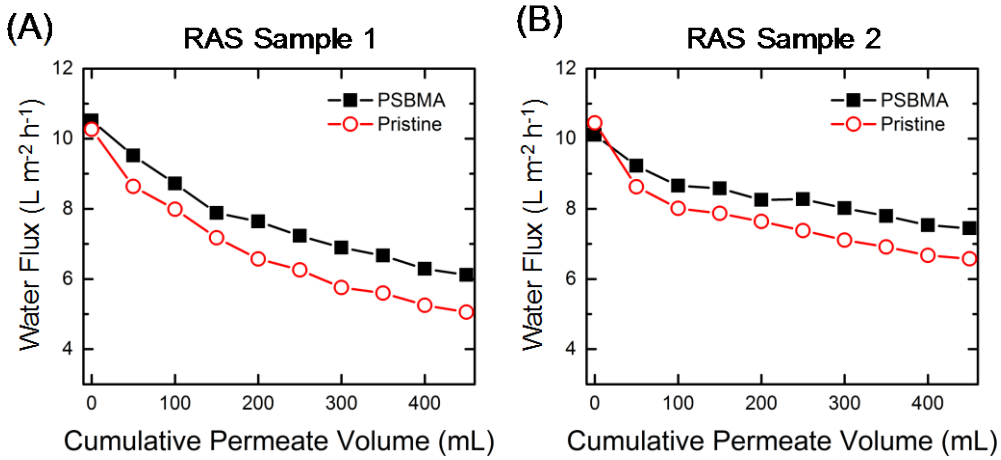

Figure 40. Water flux as a function of cumulative permeate volume for the pristine TFC and zwitterionic polymer (PSBMA)-modified TFC membranes in OsMBR using return activated sludges (RAS) as feedwater, obtained from Hyperion wastewater treatment plant located in Los Angeles, California. Results for (A) RAS sample 1 and (B) RAS sample 2. Characteristics of the RAS samples are shown in Table 1. The initial water flux was approximately 10 $L \cdot m^{-2} \cdot h^{-1}$ adjusted by an NaCl draw solution (concentration ranged from 0.19 to 0.195 M). The cross-flow velocity of the draw and feed solutions was set to be 20 cm/s. Temperature was maintained at 30.0 ± 1.0 °C.

Conclusions and Implications for Future Research

We have developed antifouling TFC membranes for use in the osmotic membrane bio-reactor (OsMBR) to treat wastewaters at forward operating bases. We proposed two different modification strategies, i*n-situ fabrication* modification and *post-fabrication* membrane modification, to chemically or physically graft antifouling materials on the membrane surface. *In-situ fabrication* modification involves fabrication of a polyamide selective layer via interfacial polymerization and anchoring jeffamine, an amine-terminated poly(ethylene glycol) derivative, onto the nascent polyamide layer by reaction with surface acyl chloride groups.

For *post-fabrication* strategy, we modified the surface of commercial TFC-FO membranes by grafting three different hydrophilic materials: (i) jeffamine, (ii) silica nanoparticles (SiNPs), and (iii) zwitterionic polymer brushes. jeffamine was bound to the membrane surface using a carbodiimide-mediated, amide coupling reaction. SiNP-based modification consists of functionalization of SiNPs using silane molecules with amine terminal groups or quaternary ammonium moieties, followed by dip-coating of the TFC membrane with the functionalized SiNPs. TFC membrane modification with zwitterionic polymer brushes was achieved by surface-initiated atom-transfer radical-polymerization (ATRP).

Our investigation revealed that the *in-situ fabrication* technique cannot guarantee consistent fouling resistance of the fabricated membranes. Because this technique involves interfacial polymerization, which is highly affected by experimental conditions such as temperature and humidity, the fabricated membranes exhibited inconsistent water permeability and salt permeability. Therefore, we concluded that unless experimental conditions are strictly controlled, *in-situ fabrication* technique may not be adequate to produce consistent and reliable fouling resistance of TFC membranes.

In contrast, the *post-fabrication* modification techniques enabled us to use commercial TFC-FO membranes, which have consistent performance properties, as substrate membranes. We successfully modified TFC membranes with three different hydrophilic materials via *post-fabrication* techniques. Furthermore, we demonstrated an enhanced fouling resistance of the modified TFC membranes in static and dynamic fouling experiments with various foulants, without impacting the intrinsic membrane transport properties.

Next, we conducted a comparative study to determine the most promising *post-fabrication* technique for antifouling TFC membranes. Specifically, we compared the efficacies of SiNP-based and zwitterionic polymer brush-based modification techniques that result in homogeneous and dense grafting of the target hydrophilic materials. We found that the zwitterionic polymer-modified membranes exhibited superior antifouling performance compared to the SiNP-modified membranes in static adsorption tests with proteins and bacteria as well as in forward osmosis fouling experiments with alginate as a model organic foulant.

To elucidate the antifouling mechanisms of the modified membranes, we carried out chemical force microscopy measurements for the control and modified membranes. Chemical force microscopy revealed that while electrostatic interactions between the foulants and the membrane surface can aggravate organic fouling, calcium ion-induced complexation of surface carboxylic groups is the primary membrane fouling mechanism. For the SiNPs-TFC membrane, enhanced hydrophilicity imparted by SiNPs can increase fouling resistance. However, the positive surface

charge of the functionalized SiNPs promotes foulant adsorption. In addition, the surface carboxylic groups on the membrane may still be accessible to foulants and thus aggravate fouling via complexation of carboxylic groups. For the PSBMA-TFC membrane, on the other hand, the net zero-charged zwitterionic polymer brushes effectively shielded the carboxylic groups on the membrane and provided steric hindrance for foulant adsorption. We conclude that these unique features render zwitterionic polymers as an excellent coating material compared to other hydrophilic materials for antifouling membrane modification.

We tested the antifouling performance of the zwitterionic polymer-modified membrane in an OsMBR with return activated sludge (RAS) as a feedwater, obtained from the Hyperion wastewater treatment plant (Los Angeles, California). The results showed that the average water flux decline was noticeably reduced (~ 34%) relative to the pristine TFC membrane (~ 44%). This increased fouling resistance in realistic operating conditions demonstrates the promise of implementation of OsMBRs equipped with zwitterionic polymer-modified membranes for wastewater treatment applications.

We emphasize that the developed technique can be easily adopted to modify large-scale FO membranes for the three following reasons. First, all the chemicals, including zwitterionic SBMA monomers, are commercially available at low price. The ARGET-ATRP polymerization method employed in our work also allows us to use 100 – 1000 times less amount of catalyst compared to traditional ATRP methods. Second, the developed technique requires simple and common equipment (e.g., plastic containers). This simplicity provides a great advantage for up-scaling, compared to other controlled polymerization methods. For example, initiated chemical vapor deposition (iCVD) requires a specialized reactor; construction of a large, complex reactor may increase the cost for large-scale membrane modification. Third, ARGET-ATRP tolerates a limited amount of oxygen. This oxygen tolerance allows for a simple reactor design, while reactors employing traditional ATRP methods need an additional mechanism for complete exclusion of oxygen.

The results of this work suggest a number of avenues for further development:

- **Optimization of the thickness of zwitterionic polymer brush layer**. The surface-initiated ATRP chemistry used in our work allows for easy control of the length of zwitterionic polymer by tuning the duration of polymerization. This controllability will enable us to optimize the polymerization duration such that modified membranes exhibit highly effective antifouling performance while minimizing the impact on membrane transport properties (water flux and salt rejection).
- **Development of an alternative method to achieve a high surface density of initiator**. Effective antifouling surfaces require a dense grafting of zwitterionic polymer brushes. This necessitates a high surface density of initiators immobilized on the membranes surface. Although the surface density of initiators can be increased by deposition of a thicker PDA layer, such a thick PDA layer will significantly compromise the membrane transport properties. Since the polyamide active layer of TFC membranes is relatively inert and therefore difficult to chemically modify, an alternative route to immobilize initiators without using a PDA layer is highly desired for dense grafting of zwitterionic polymer brushes, without affecting water and salt permeabilities.

- **Expanding the developed zwitterionic polymer coating by incorporating other functional materials**. Despite the antifouling performance of the zwitterionic polymer-modified membrane shown in the OsMBR test (Figure 41), the fouling resistance could be further improved by integrating antifouling and antimicrobial materials on TFC membranes. Actual feedwaters treated in OsBMRs, such as RAS, will likely induce biofouling. The static adsorption test using *E. coli* (Figure 37) clearly indicates that the zwitterionic polymer-modified membrane effectively prevents adsorption of microorganisms due to the highly hydrophilic nature, steric hindrance by swelling, and suppressed electrostatic interactions. However, due to the advection of feedwater toward the membrane by the permeate flow and foulant rejection by the active layer, the membrane surface is continuously exposed to more highly concentrated foulants (including bacteria) than those present in the bulk. Once foulants adsorb to the membrane surface, the aforementioned antifouling mechanisms cannot be effective and instead the dominant interaction occurs between the newly approaching foulants and the already deposited foulants. Without any bactericidal mechanism provided, bacteria and other microorganisms in the feed water may proliferate on the adsorbed foulant layer and eventually result in biofouling.

Appendices

Table A1. Summary of flux decline data for dynamic organic fouling experiments using sodium chloride draw solution

	Initial Flux, $J_{w,0}$	**Final Flux, $J_{w,500mL}$**	**Flux Decline due to Fouling, FD_{500mL}**	**Flux Recovery after Cleaning, %**
Control Membrane				
Baseline	20.5 LMH	17.9 LMH	20.8%	86.8%
Fouling	20.4 LMH	14.1 LMH		
Recovery	17.8 LMH	11.2 LMH		
Control Membrane				
Baseline	20.3 LMH	16.4 LMH	27.8%	97.0%
Fouling	20.4 LMH	11.9 LMH		
Recovery	19.7 LMH	12.4 LMH		
2% jeffamine Membrane				
Baseline	20.6 LMH	16.4 LMH	16.7%	100%
Fouling	20.2 LMH	13.4 LMH		
Recovery	20.6 LMH	13.2 LMH		
2% jeffamine Membrane				
Baseline	20.3 LMH	15.2 LMH	2.5%	90.1%
Fouling	20.0 LMH	14.6 LMH		
Recovery	18.3 LMH	14.5 LMH		
2% jeffamine Membrane				
Baseline	18.6 LMH	16.4 LMH	13.7%	101%
Fouling	18.8 LMH	14.3 LMH		
Recovery	18.8 LMH	14.8 LMH		

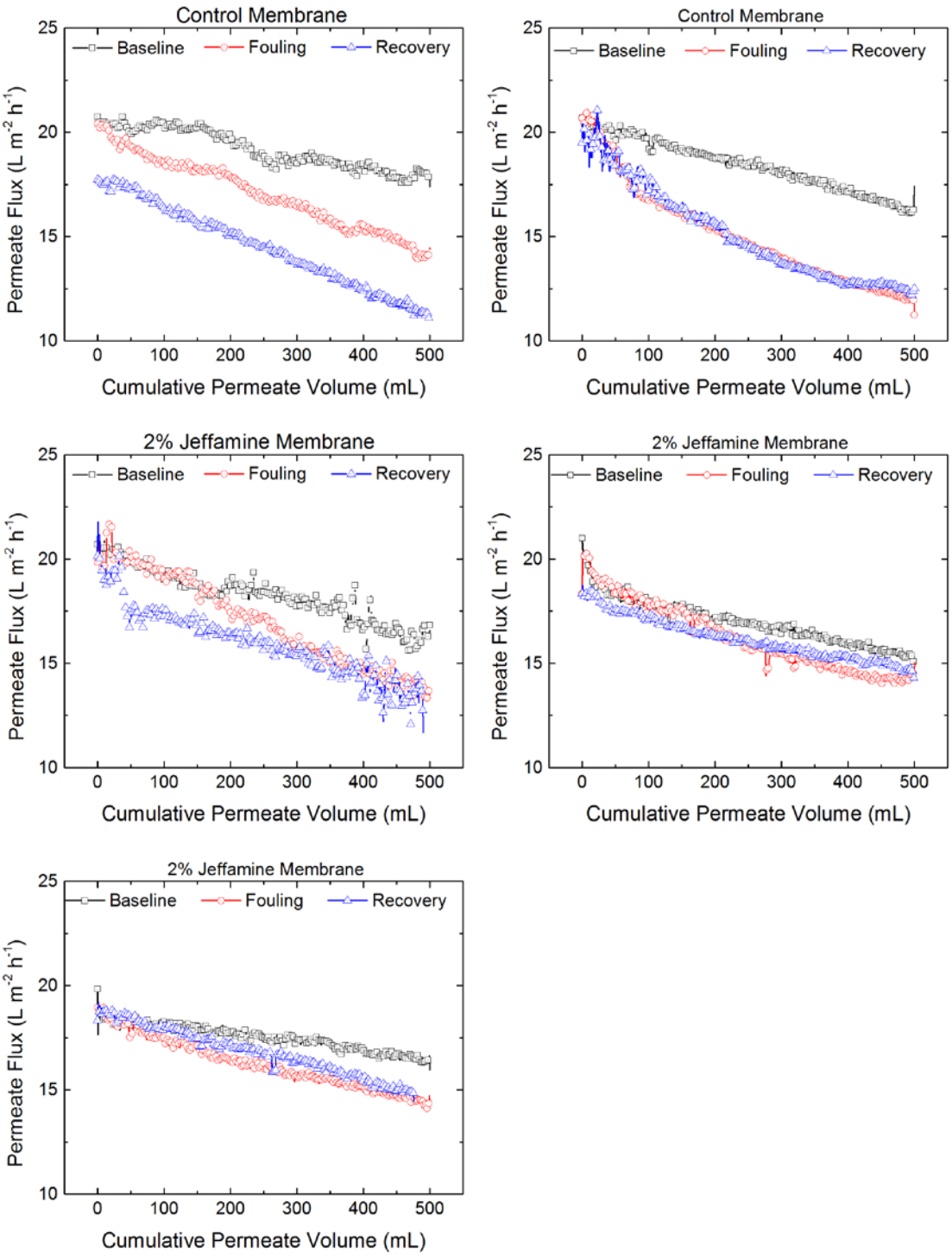

Figure A1. Permeate flux decline curves for the baseline, fouling, and recovery portions of dynamic fouling experiments conducted with sodium chloride draw solution for control and 2% jeffamine modified membranes.

Table A2. Summary of flux decline data for dynamic organic fouling experiments using magnesium chloride draw solution

	Initial Flux, $J_{w,0}$	**Final Flux, $J_{w,500mL}$**	**Flux Decline due to Fouling, FD_{500mL}**	**Flux Recovery after Cleaning, %**
Control Membrane				
Baseline	16.3 LMH	14.4 LMH	23.6 %	114%
Fouling	16.6 LMH	11.2 LMH		
Recovery	18.6 LMH	15.8 LMH		
Control Membrane				
Baseline	16.5 LMH	14.7 LMH	25.8 %	113%
Fouling	16.8 LMH	11.1 LMH		
Recovery	18.6 LMH	15.9 LMH		
Control Membrane				
Baseline	20.4 LMH	18.2 LMH	30.9 %	126%
Fouling	22.4 LMH	13.8 LMH		
Recovery	25.8 LMH	21.9 LMH		
2% jeffamine Membrane				
Baseline	15.9 LMH	13.6 LMH	11.0 %	102%
Fouling	15.1 LMH	11.5 LMH		
Recovery	16.2 LMH	14.3 LMH		
2% jeffamine Membrane				
Baseline	18.2 LMH	14.7 LMH	6.8 %	98.4%
Fouling	17.0 LMH	12.8 LMH		
Recovery	17.9 LMH	15.7 LMH		

Literature Cited

[1] B. Mi, M. Elimelech, Chemical and physical aspects of organic fouling of forward osmosis membranes, J Membrane Sci, 320 (2008) 292-302.
[2] A. Tiraferri, N.Y. Yip, W.A. Phillip, J.D. Schiffman, M. Elimelech, Relating performance of thin-film composite forward osmosis membranes to support layer formation and structure, J Membrane Sci, 367 (2011) 340-352.
[3] L.A.S. Hoover, J. D.; Elimelech, M. , Fabrication of thin-film composite membranes on electrospun poly(ethylene terephthalate) (PET) for engineered osmosis, in: 22nd Annual Meeting of the North American Membrane Society, New Orleans, LA, 2012.
[4] A. Tiraferri, N.Y. Yip, A.P. Straub, S. Romero-Vargas Castrillon, M. Elimelech, A method for the simultaneous determination of transport and structural parameters of forward osmosis membranes, Journal of Membrane Science, 444 (2013) 523-538.
[5] L.A. Hoover, W.A. Phillip, A. Tiraferri, N.Y. Yip, M. Elimelech, Forward with Osmosis: Emerging Applications for Greater Sustainability, Environ Sci Technol, 45 (2011) 9824-9830.
[6] J.R. McCutcheon, M. Elimelech, Influence of concentrative and dilutive internal concentration polarization on flux behavior in forward osmosis, J Membrane Sci, 284 (2006) 237-247.
[7] T.Y. Cath, A.E. Childress, M. Elimelech, Forward osmosis: Principles, applications, and recent developments, J Membrane Sci, 281 (2006) 70-87.
[8] R.E. Kravath, J.A. Davis, Desalination of Sea-Water by Direct Osmosis, Desalination, 16 (1975) 151-155.
[9] T.Y. Cath, D. Adams, A.E. Childress, Membrane contactor processes for wastewater reclamation in space II. Combined direct osmosis, osmotic distillation, and membrane distillation for treatment of metabolic wastewater, J Membrane Sci, 257 (2005) 111-119.
[10] B. Jiao, A. Cassano, E. Drioli, Recent advances on membrane processes for the concentration of fruit juices: a review, J Food Eng, 63 (2004) 303-324.
[11] E.M. Garcia-Castello, J.R. McCutcheon, M. Elimelech, Performance evaluation of sucrose concentration using forward osmosis, J Membrane Sci, 338 (2009) 61-66.
[12] A. Achilli, T.Y. Cath, E.A. Marchand, A.E. Childress, The forward osmosis membrane bioreactor: A low fouling alternative to MBR processes, Desalination, 239 (2009) 10-21.
[13] B.X. Mi, M. Elimelech, Organic fouling of forward osmosis membranes: Fouling reversibility and cleaning without chemical reagents, J Membrane Sci, 348 (2010) 337-345.
[14] Q.L. Li, M. Elimelech, Organic fouling and chemical cleaning of nanofiltration membranes: Measurements and mechanisms, Environ Sci Technol, 38 (2004) 4683-4693.
[15] M. Morra, On the molecular basis of fouling resistance, J Biomat Sci-Polym E, 11 (2000) 547-569.
[16] A. Tiraferri, Y. Kang, E.P. Giannelis, M. Elimelech, Highly Hydrophilic Thin-Film Composite Forward Osmosis Membranes Functionalized with Surface-Tailored Nanoparticles, Acs Appl Mater Inter, 4 (2012) 5044-5053.
[17] K.L. Prime, G.M. Whitesides, Self-Assembled Organic Monolayers - Model Systems for Studying Adsorption of Proteins at Surfaces, Science, 252 (1991) 1164-1167.
[18] R.G. Chapman, E. Ostuni, S. Takayama, R.E. Holmlin, L. Yan, G.M. Whitesides, Surveying for surfaces that resist the adsorption of proteins, J Am Chem Soc, 122 (2000) 8303-8304.

[19] E.M. Van Wagner, A.C. Sagle, M.M. Sharma, Y.H. La, B.D. Freeman, Surface modification of commercial polyamide desalination membranes using poly(ethylene glycol) diglycidyl ether to enhance membrane fouling resistance, J Membrane Sci, 367 (2011) 273-287.
[20] A. Tiraferri, Y. Kang, E.P. Giannelis, M. Elimelech, Superhydrophilic Thin-Film Composite Forward Osmosis Membranes for Organic Fouling Control: Fouling Behavior and Antifouling Mechanisms, Environ Sci Technol, 46 (2012) 11135-11144.
[21] R. Zhang, Y. Liu, M. He, Y. Su, X. Zhao, M. Elimelech, Z. Jiang, Antifouling membranes for sustainable water purification: strategies and mechanisms, Chemical Society reviews, 45 (2016) 5888-5924.
[22] N.Y. Yip, A. Tiraferri, W.A. Phillip, J.D. Schiffman, M. Elimelech, High Performance Thin-Film Composite Forward Osmosis Membrane, Environ Sci Technol, 44 (2010) 3812-3818.
[23] G.D. Kang, M. Liu, B. Lin, Y.M. Cao, Q. Yuan, A novel method of surface modification on thin-film composite reverse osmosis membrane by grafting poly(ethylene glycol), Polymer, 48 (2007) 1165-1170.
[24] A. Tiraferri, Y. Kang, E.P. Giannelis, M. Elimelech, Highly hydrophilic thin-film composite forward osmosis membranes functionalized with surface-tailored nanoparticles, ACS applied materials & interfaces, 4 (2012) 5044-5053.
[25] M. Herzberg, M. Elimelech, Biofouling of reverse osmosis membranes: Role of biofilm-enhanced osmotic pressure, J Membrane Sci, 295 (2007) 11-20.
[26] G. Kang, H. Yu, Z. Liu, Y. Cao, Surface modification of a commercial thin film composite polyamide reverse osmosis membrane by carbodiimide-induced grafting with poly(ethylene glycol) derivatives, Desalination, 275 (2011) 252-259.
[27] E.M. Van Wagner, A.C. Sagle, M.M. Sharma, Y.-H. La, B.D. Freeman, Surface modification of commercial polyamide desalination membranes using poly(ethylene glycol) diglycidyl ether to enhance membrane fouling resistance, Journal of Membrane Science, 367 (2011) 273-287.
[28] L. Zou, I. Vidalis, D. Steele, A. Michelmore, S.P. Low, J.Q.J.C. Verberk, Surface hydrophilic modification of RO membranes by plasma polymerization for low organic fouling, Journal of Membrane Science, 369 (2011) 420-428.
[29] X. Lu, S. Romero-Vargas Castrillón, D.L. Shaffer, J. Ma, M. Elimelech, In Situ Surface Chemical Modification of Thin-Film Composite Forward Osmosis Membranes for Enhanced Organic Fouling Resistance, Environmental science & technology, 47 (2013) 12219-12228.
[30] S. Romero-Vargas Castrillón, X. Lu, D.L. Shaffer, M. Elimelech, Amine enrichment and poly(ethylene glycol) (PEG) surface modification of thin-film composite forward osmosis membranes for organic fouling control, Journal of Membrane Science, 450 (2014) 331-339.
[31] D. Rana, T. Matsuura, Surface modifications for antifouling membranes, Chemical reviews, 110 (2010) 2448-2471.
[32] G.-d. Kang, Y.-m. Cao, Development of antifouling reverse osmosis membranes for water treatment: A review, Water Research, 46 (2012) 584-600.
[33] C.Y. Tang, Y.-N. Kwon, J.O. Leckie, Probing the nano- and micro-scales of reverse osmosis membranes—A comprehensive characterization of physiochemical properties of uncoated and coated membranes by XPS, TEM, ATR-FTIR, and streaming potential measurements, Journal of Membrane Science, 287 (2007) 146-156.
[34] V. Freger, J. Gilron, S. Belfer, TFC polyamide membranes modified by grafting of hydrophilic polymers: an FT-IR/AFM/TEM study, Journal of Membrane Science, 209 (2002) 283-292.

[35] G. Kang, M. Liu, B. Lin, Y. Cao, Q. Yuan, A novel method of surface modification on thin-film composite reverse osmosis membrane by grafting poly(ethylene glycol), Polymer, 48 (2007) 1165-1170.
[36] Y.-N. Kwon, J.O. Leckie, Hypochlorite degradation of crosslinked polyamide membranes: II. Changes in hydrogen bonding behavior and performance, Journal of Membrane Science, 282 (2006) 456-464.
[37] I. Noda, A. Dowrey, J. Haynes, C. Marcott, Group frequency assignments for major infrared bands observed in common synthetic polymers, in: Physical Properties of Polymers Handbook, Springer, 2007, pp. 395-406.
[38] O. Coronell, M.I. González, B.J. Mariñas, D.G. Cahill, Ionization Behavior, Stoichiometry of Association, and Accessibility of Functional Groups in the Active Layers of Reverse Osmosis and Nanofiltration Membranes, Environmental Science & Technology, 44 (2010) 6808-6814.
[39] ISO, 4287: Geometrical Product Specifications (GPS)-Surface texture: Profile method–Terms, definitions and surface texture parameters, in, International Organization for Standardization, 1997.
[40] S. Lee, C. Boo, M. Elimelech, S. Hong, Comparison of fouling behavior in forward osmosis (FO) and reverse osmosis (RO), Journal of Membrane Science, 365 (2010) 34-39.
[41] C.Y. Tang, Q. She, W.C.L. Lay, R. Wang, A.G. Fane, Coupled effects of internal concentration polarization and fouling on flux behavior of forward osmosis membranes during humic acid filtration, Journal of Membrane Science, 354 (2010) 123-133.
[42] B. Mi, M. Elimelech, Chemical and physical aspects of organic fouling of forward osmosis membranes, Journal of Membrane Science, 320 (2008) 292-302.
[43] D.L. Shaffer, J.R. Werber, H. Jaramillo, S. Lin, M. Elimelech, Forward osmosis: Where are we now?, Desalination, 356 (2015) 271-284.
[44] S. Lee, M. Elimelech, Relating Organic Fouling of Reverse Osmosis Membranes to Intermolecular Adhesion Forces, Environmental science & technology, 40 (2006) 980-987.
[45] J.N. Israelachvili, 11 - Contrasts between Intermolecular, Interparticle, and Intersurface Forces, in: Intermolecular and Surface Forces (Third Edition), Academic Press, Boston, 2011, pp. 205-222.
[46] V. Freger, Nanoscale Heterogeneity of Polyamide Membranes Formed by Interfacial Polymerization, Langmuir, 19 (2003) 4791-4797.
[47] F.A. Pacheco, I. Pinnau, M. Reinhard, J.O. Leckie, Characterization of isolated polyamide thin films of RO and NF membranes using novel TEM techniques, Journal of Membrane Science, 358 (2010) 51-59.
[48] G. Ye, J. Lee, F. Perreault, M. Elimelech, Controlled Architecture of Dual-Functional Block Copolymer Brushes on Thin-Film Composite Membranes for Integrated "Defending" and "Attacking" Strategies against Biofouling, ACS applied materials & interfaces, 7 (2015) 23069-23079.
[49] A.-h.M.A. El-Aassar, Polyamide Thin Film Composite Membranes Using Interfacial Polymerization: Synthesis, Characterization and Reverse Osmosis Performance for Water Desalination, Australian Journal of Basic and Applied Sciences, 6 (2012) 382-391.
[50] B. Zhu, S. Edmondson, Polydopamine-melanin initiators for Surface-initiated ATRP, Polymer, 52 (2011) 2141-2149.
[51] J.B. Schlenoff, Zwitteration: coating surfaces with zwitterionic functionality to reduce nonspecific adsorption, Langmuir : the ACS journal of surfaces and colloids, 30 (2014) 9625-9636.

[52] A.E. Childress, M. Elimelech, Effect of solution chemistry on the surface charge of polymeric reverse osmosis and nanofiltration membranes, Journal of Membrane Science, 119 (1996) 253-268.
[53] A. Tiraferri, M. Elimelech, Direct quantification of negatively charged functional groups on membrane surfaces, Journal of Membrane Science, 389 (2012) 499-508.
[54] W. Guo, H.-H. Ngo, J. Li, A mini-review on membrane fouling, Bioresource Technology, 122 (2012) 27-34.
[55] I. Banerjee, R.C. Pangule, R.S. Kane, Antifouling coatings: recent developments in the design of surfaces that prevent fouling by proteins, bacteria, and marine organisms, Advanced materials, 23 (2011) 690-718.
[56] A.J. de Kerchove, P. Weroński, M. Elimelech, Adhesion of Nonmotile Pseudomonas aeruginosa on "Soft" Polyelectrolyte Layer in a Radial Stagnation Point Flow System: Measurements and Model Predictions, Langmuir : the ACS journal of surfaces and colloids, 23 (2007) 12301-12308.
[57] K. Nakanishi, T. Sakiyama, K. Imamura, On the adsorption of proteins on solid surfaces, a common but very complicated phenomenon, J Biosci Bioeng, 91 (2001) 233-244.
[58] M. Teixido, J.J. Pignatello, J.L. Beltran, M. Granados, J. Peccia, Speciation of the Ionizable Antibiotic Sulfamethazine on Black Carbon (Biochar), Environ Sci Technol, 45 (2011) 10020-10027.
[59] W.S. Ang, A. Tiraferri, K.L. Chen, M. Elimelech, Fouling and cleaning of RO membranes fouled by mixtures of organic foulants simulating wastewater effluent, Journal of Membrane Science, 376 (2011) 196-206.
[60] W.S. Ang, N.Y. Yip, A. Tiraferri, M. Elimelech, Chemical cleaning of RO membranes fouled by wastewater effluent: Achieving higher efficiency with dual-step cleaning, Journal of Membrane Science, 382 (2011) 100-106.
[61] G.T. Grant, E.R. Morris, D.A. Rees, P.J.C. Smith, D. Thom, Biological interactions between polysaccharides and divalent cations: The egg-box model, FEBS Letters, 32 (1973) 195-198.
[62] X. Zhu, M. Elimelech, Colloidal Fouling of Reverse Osmosis Membranes: Measurements and Fouling Mechanisms, Environmental science & technology, 31 (1997) 3654-3662.
[63] G.D. Kang, Y.M. Cao, Development of antifouling reverse osmosis membranes for water treatment: A review, Water research, 46 (2012) 584-600.
[64] M. Hadidi, A.L. Zydney, Fouling behavior of zwitterionic membranes: Impact of electrostatic and hydrophobic interactions, Journal of Membrane Science, 452 (2014) 97-103.
[65] A. Tiraferri, Y. Kang, E.P. Giannelis, M. Elimelech, Superhydrophilic thin-film composite forward osmosis membranes for organic fouling control: fouling behavior and antifouling mechanisms, Environmental science & technology, 46 (2012) 11135-11144.
[66] A.J. de Kerchove, M. Elimelech, Impact of Alginate Conditioning Film on Deposition Kinetics of Motile and Nonmotile Pseudomonas aeruginosa Strains, Applied and Environmental Microbiology, 73 (2007) 5227-5234.
[67] J.E. Rosen, F.X. Gu, Surface Functionalization of Silica Nanoparticles with Cysteine: A Low-Fouling Zwitterionic Surface, Langmuir : the ACS journal of surfaces and colloids, 27 (2011) 10507-10513.
[68] S. Jiang, Z. Cao, Ultralow-fouling, functionalizable, and hydrolyzable zwitterionic materials and their derivatives for biological applications, Advanced materials, 22 (2010) 920-932.

[69] C. Leng, H.-C. Hung, S. Sun, D. Wang, Y. Li, S. Jiang, Z. Chen, Probing the Surface Hydration of Nonfouling Zwitterionic and PEG Materials in Contact with Proteins, ACS applied materials & interfaces, 7 (2015) 16881-16888.
[70] B.Q. Liao, D.M. Bagley, H.E. Kraemer, G.G. Leppard, S.N. Liss, A Review of Biofouling and its Control in Membrane Separation Bioreactors, Water Environment Research, 76 (2004) 425-436.
[71] D. Johnson, N. Hilal, Characterisation and quantification of membrane surface properties using atomic force microscopy: A comprehensive review, Desalination, 356 (2015) 149-164.
[72] C.H. Liu, A.F. Faria, J. Ma, M. Elimelech, Mitigation of Biofilm Development on Thin-Film Composite Membranes Functionalized with Zwitterionic Polymers and Silver Nanoparticles, Environ Sci Technol, 51 (2017) 182-191.